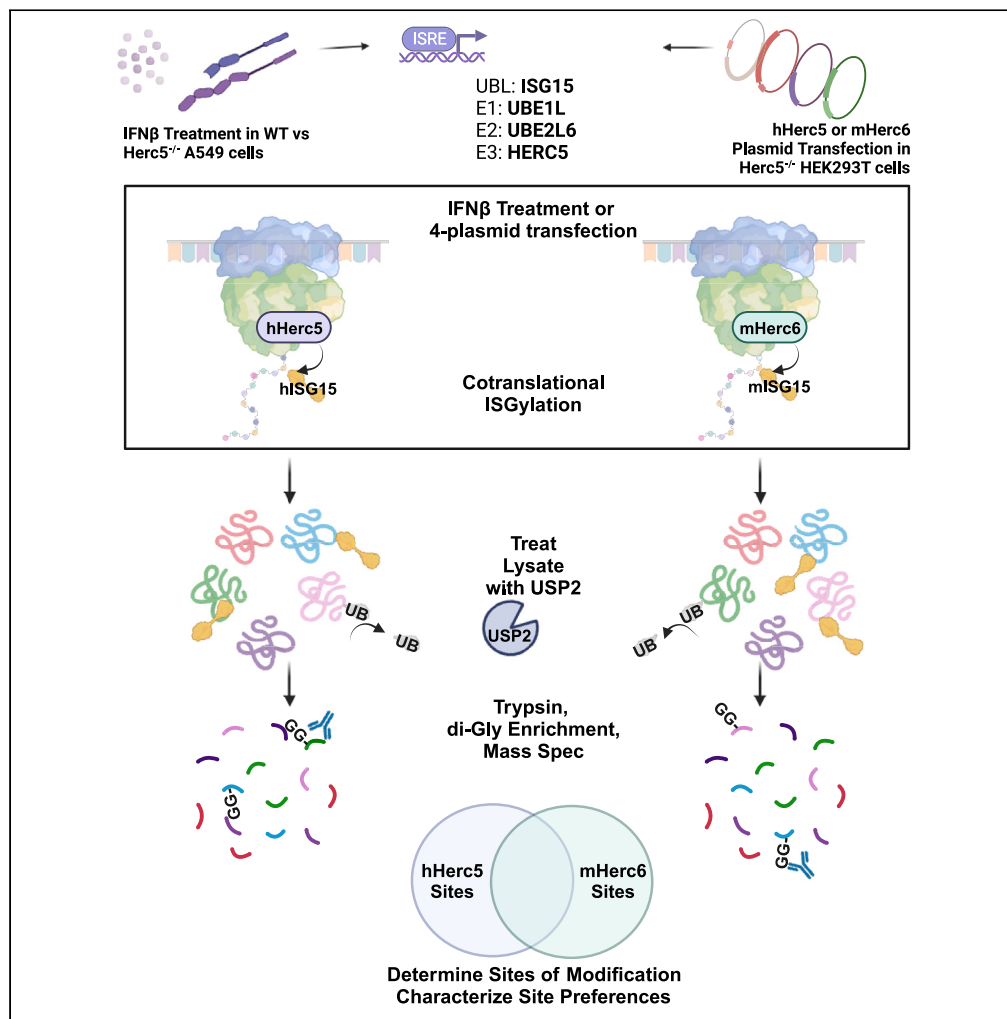


Article

# Cellular targets and lysine selectivity of the HERC5 ISG15 ligase



Xu Zhao, Jessica M. Perez, Peter A. Faull, ..., Larissa A. Canadeo, Can Cenik, Jon M. Huibregtse

huibregtse@austin.utexas.edu

Highlights

The human (hHERC5) and mouse (mHERC6) ISG15 ligases are ribosome associated

>7,000 hHERC5 and mHERC6 modification sites were identified in >2,700 proteins

hHERC5 and mHERC6 differ in their lysine selectivity based on sequence context

ISGylation sites for both enzymes were consistent with cotranslational ISGylation

Zhao et al., iScience 27, 108820  
February 16, 2024 © 2024 The Authors.  
<https://doi.org/10.1016/j.isci.2024.108820>



## Article

## Cellular targets and lysine selectivity of the HERC5 ISG15 ligase

Xu Zhao,<sup>1,4</sup> Jessica M. Perez,<sup>1</sup> Peter A. Faull,<sup>2,5</sup> Catherine Chan,<sup>1</sup> Femke W. Munting,<sup>1</sup> Larissa A. Canadeo,<sup>1</sup> Can Cenik,<sup>1</sup> and Jon M. Huibregtse<sup>1,3,6,\*</sup>

## SUMMARY

**ISG15 is a type I interferon-induced ubiquitin-like modifier that functions in innate immune responses. The major human ISG15 ligase is hHERC5, a ribosome-associated HECT E3 that broadly ISGylates proteins cotranslationally. Here, we characterized the hHERC5-dependent ISGylome and identified over 2,000 modified lysines in over 1,100 proteins in IFN- $\beta$ -stimulated cells. In parallel, we compared the substrate selectivity hHERC5 to the major mouse ISG15 ligase, mHERC6, and analysis of sequences surrounding ISGylation sites revealed that hHERC5 and mHERC6 have distinct preferences for amino acid sequence context. Several features of the datasets were consistent with ISGylation of ribosome-tethered nascent chains, and mHERC6, like hHERC5, cotranslationally modified nascent polypeptides. The ISGylome datasets presented here represent the largest numbers of protein targets and modification sites attributable to a single Ub/Ubl ligase and the lysine selectivities of the hHERC5 and mHERC6 enzymes may have implications for the activities of HECT domain ligases, generally.**

## INTRODUCTION

Type 1 interferon (IFN- $\alpha/\beta$ ) signaling leads to the expression of hundreds of interferon-stimulated genes (ISGs) in vertebrate cells, and the protein products of these genes play important roles in the innate immune response to viral and microbial pathogens, either as effector proteins or regulators of the interferon response.<sup>1</sup> Importantly, the functions and mechanisms of only a small number of the effector proteins are understood in molecular detail. Some of the better characterized effectors include MxA, OAS/RNaseL, TRIM proteins, IFITM, viperin, and tetherin, each of which interferes with one or more aspects of virus ingress or egress, genome replication, or vRNA function or stability.<sup>2,3</sup> ISG15 was one of the first ISGs to be discovered as well as the first ubiquitin-like protein modifier (Ubl) to be discovered after ubiquitin.<sup>4-6</sup> Human ISG15 is a 157 amino acid (~17 kD) protein and consists of two ubiquitin-like domains separated by a short flexible linker. Each of the domains is less than 40% identical to ubiquitin, and ISG15 sequences diverge significantly among mammalian species. For example, human and mouse ISG15 are approximately 66% identical, and mouse (*Mus musculus*) and rat (*Rattus rattus*) ISG15 are approximately 73% identical.

Like other UbIs, ISG15 conjugation requires a cooperating set of E1, E2, and E3 enzymes. The human ISG15 E1 and E2 proteins are UBA7/UBE1L and UBE2L6/UBCH8, respectively.<sup>7-9</sup> The major ISG15 E3 ligase in human cells is HERC5 (hHERC5),<sup>10</sup> a HECT domain ligase and the only one of the 28 human HECT E3 that is known to conjugate a Ubl other than ubiquitin. Depletion of hHERC5 abrogates nearly all ISGylation in IFN- $\beta$ -stimulated cells, and co-expression of ISG15, UBA7, UBE2L6, and hHERC5 in non-IFN-treated cells recapitulates ISGylation of target proteins.<sup>10</sup> The *UBA7*, *UBE2L6*, and *HERC5* genes are, like *ISG15*, induced at the transcriptional level by type I IFN signaling and are therefore also ISGs.<sup>10</sup> Two other E3s have been reported to function in ISGylation (TRIM25/EFP and ARIH1/HHARI), although these appear to have a very small number of substrates and may play highly specialized roles in ISGylation.<sup>11,12</sup> Interestingly, the human *HERC6* gene, which is also transcriptionally activated by type 1 IFN signaling, is adjacent to *HERC5* on chromosome 4 and the hHERC6 and hHERC5 proteins have a similar protein domain organization.<sup>13</sup> Both contain a series of N-terminal RCC1 repeats (spanning approximately 370 amino acids), a central region of approximately 270 amino acids predicted to consist primarily of a series of stacked alpha helices (based on AlphaFold<sup>14</sup> prediction), and a C-terminal HECT domain of approximately 380 amino acids. Despite these similarities, hHERC6 does not appear to play a significant or perhaps any role in ISG15 conjugation in human cells. However, mice completely lack a *HERC5* gene, and *HERC6* (mHERC6) is the major ISG15 ligase in mice.<sup>15-17</sup> Most other rodents are like mice in this regard (i.e., possessing a *HERC6* gene and lacking a *HERC5* gene), but this gene organization is rare outside of rodents, with the only other reported example being the white rhinoceros, *Ceratotherium simum*.<sup>15,17</sup> In

<sup>1</sup>Department of Molecular Biosciences, University of Texas at Austin, Austin, TX 78712, USA

<sup>2</sup>Biological Mass Spectrometry Facility, Center for Biomedical Research Support, University of Texas at Austin, Austin, TX 78712, USA

<sup>3</sup>John Ring LaMontagne Center for Infectious Disease, University of Texas at Austin, Austin, TX 78712, USA

<sup>4</sup>Present address: The Broad Institute, 415 Main St., Cambridge, MA 02142, USA

<sup>5</sup>Present address: Northwestern Proteomics Core Facility, Northwestern University, Chicago, IL 60611, USA

<sup>6</sup>Lead contact

\*Correspondence: [huibregtse@austin.utexas.edu](mailto:huibregtse@austin.utexas.edu)

<https://doi.org/10.1016/j.isci.2024.108820>



contrast, cetaceans (dolphins and whales) have a *HERC5* gene but do not have an intact *HERC6* gene, while a small number of species (chinchilla and the little brown bat, *Myotis lucifugus*) have both a *HERC5* and *HERC6* gene with an additional gene that resembles a *HERC5/HERC6* chimera, located directly between their *HERC5* and *HERC6* genes.<sup>13</sup> This surprising variation at the *HERC5/HERC6* loci is consistent with the fact that both the *HERC5* and *HERC6* genes, like many other genes encoding components of the innate immune response, are rapidly evolving genes and under positive genetic selection.<sup>13,18</sup> This is generally interpreted as an indicator of an evolutionary “arms race” between host and pathogens. It should be noted that among mammalian *HERC5* and *HERC6* proteins, ISG15 ligase activities have, to our knowledge, only been experimentally validated and reported for human *HERC5* and mouse *HERC6*.

Although ISG15-deficient mice exhibit an increased susceptibility to many viral infections,<sup>19</sup> a single general biochemical function of protein ISGylation remains unclear and it does not target proteins for proteasomal degradation. Early proteomics studies identified over 300 cellular proteins as substrates for ISGylation,<sup>20–22</sup> but their identities shed little light on the function or ISGylation. More recent studies have greatly expanded the number of potential substrates of ISGylation,<sup>23–27</sup> raising the question of how a single ligase (e.g., hHERC5 or mHERC6) can recognize such a large number of target proteins. An apparent solution to this problem came with the finding that hHERC5 associates with polyribosomes and ISGylates newly synthesized proteins in a cotranslational manner.<sup>28</sup> The N-terminal RCC1-like repeats of hHERC5 are essential for ribosome association and target protein ISGylation.<sup>28</sup> This suggested a model in which ribosome-tethered *HERC5* broadly modifies ribosome-associated nascent polypeptides in a near-stochastic manner, accounting for how a single ligase could be responsible for modifying such a large number of target proteins. We further proposed that, in the context of a viral infection and a type I interferon response, newly translated viral proteins may represent the key biologically important targets of ISG15, with covalent attachment of ISG15 functioning as a general steric inhibitor of viral protein function. Newly translated cellular proteins would also be ISGylated during an IFN response, but this may be largely collateral damage in an attempt to target and interfere with viral protein function. As ISGylation is relatively inefficient, with, in most cases, only 5%–10% of the total pool of a newly translated protein being ISGylated, viral structural proteins (e.g., capsid and nucleocapsid proteins) might be expected to be particularly sensitive to the effects of ISGylation due to dominant-negative effects on formation of oligomeric complexes. This concept has been tested in two systems: (1) a human papillomavirus pseudovirus system, where low-level ISGylation of the L1 capsid protein had a dominant-negative effect on infectivity of virus-like particles,<sup>28</sup> and (2) in an influenza B system, where the ISGylated form of the influenza B ribonucleoprotein (NP) prevented oligomerization of NP along the viral RNA.<sup>29</sup> Interestingly, the effect on NP is countered by the influenza B NS1 protein, which binds and sequesters ISGylated proteins, including ISGylated NP. It was proposed that this effectively removes ISGylated NP from the total pool of NP protein capable of oligomerizing along viral RNA.<sup>29</sup> Strong additional evidence supporting an antiviral function of ISGylation is that several virus types—including MERS, SARS-CoV-1, SARS-CoV-2, Crimean-Congo hemorrhagic fever virus, and foot-and-mouth disease virus (FMDV)—overcome the effects of ISGylation by encoding their own ISG15 deconjugating enzymes.<sup>30–35</sup> In the case of the beta coronaviruses, the de-ISGylating enzymatic activity (e.g., the PLpro domain of the nsp3 protein of SARS-CoV-2) also proteolytically processes the orf1a viral polyprotein. The dual functions of PLpro (polyprotein cleavage and de-ISGylation) are reflected in the similarity of the polyprotein cleavage sites (e.g., RLKGG for the nsp2-3 cleavage site) to the C-terminal sequence of ISG15 (RLRGG). PLpro inhibitors are attractive antiviral drug targets<sup>36</sup> as these would be expected to block both polyprotein cleavage and de-ISGylation.

The goal of the work described here was to broadly characterize the hHERC5-dependent ISGylome and to compare the activities of hHERC5 and mHERC6 in terms of cellular substrates, the sites of modification within these substrates, and characteristics of the modified proteins. While this goal may seem at odds with the hypothesis that viral rather than cellular proteins are the biologically relevant substrates of ISG15, the premise was that analysis of a large set of ISGylation sites would reveal preferred modification sites based on sequence context and position within proteins. Such preferences or biases in hHERC5 and mHERC6 modification sites might be expected to represent evolutionary adaptations to species-specific pathogen challenges. Taking advantage of the fact that the last six residues of ISG15 are identical to those of ubiquitin (LRLRGG), we used a proteomics approach previously used for global identification of ubiquitylation sites, based on antibody recognition of the K-ε-GG remnant left on modified lysines after tryptic cleavage.<sup>37,38</sup> We present an analysis of hHERC5-dependent ISGylation sites and a comparison to sites modified by mHERC6, showing that the two enzymes have distinct lysine preferences based on local sequence context. We also show that features of both the hHERC5 and mHERC6 datasets are consistent with cotranslational ISGylation of target proteins. In addition, the hHERC5 and mHERC6 ISGylomes described here represent the largest number of targets and modification sites attributable to a single ubiquitin or Ubl ligase, and these results may have implications for reactions catalyzed by HECT ubiquitin ligases, generally.

## RESULTS

### The hHERC5-dependent ISGylome in IFN-β-treated cells

A strategy for defining the hHERC5-dependent ISGylome was developed based on antibody recognition of the di-glycine (di-G) remnant left on ISGylated lysine residues following tryptic digestion, as originally developed for ubiquitin proteomics.<sup>37,38</sup> This approach was feasible because ISG15, like ubiquitin and Nedd8, terminates in an RGG sequence. An antibody specific to di-G-substituted lysine chains (anti-K-ε-GG antibodies) is available (Cell Signaling Technology) that can be used to immunoprecipitate the modified peptides, which are then identified by mass spectrometry methods. For hHERC5-specific ISG15 di-G proteomics, the challenge is to specifically identify the K-ε-GG peptides derived from hHERC5-dependent ISG15 conjugates, while eliminating peptides derived from ubiquitylated and Neddylated proteins.

Our initial approach utilized a control A549 cell line (human lung adenocarcinoma) in which *HERC5* was disrupted by CRISPR (A549-*HERC5*<sup>KO</sup>). An immunoblot of total cell lysate from IFN-β-treated cells confirmed the loss of *HERC5* expression in the A549-*HERC5*<sup>KO</sup> as well as the loss of the vast majority of ISG15 conjugates in IFN-β-treated A549-*HERC5*<sup>KO</sup> cells compared to the parental A549 cells (Figure 1A).

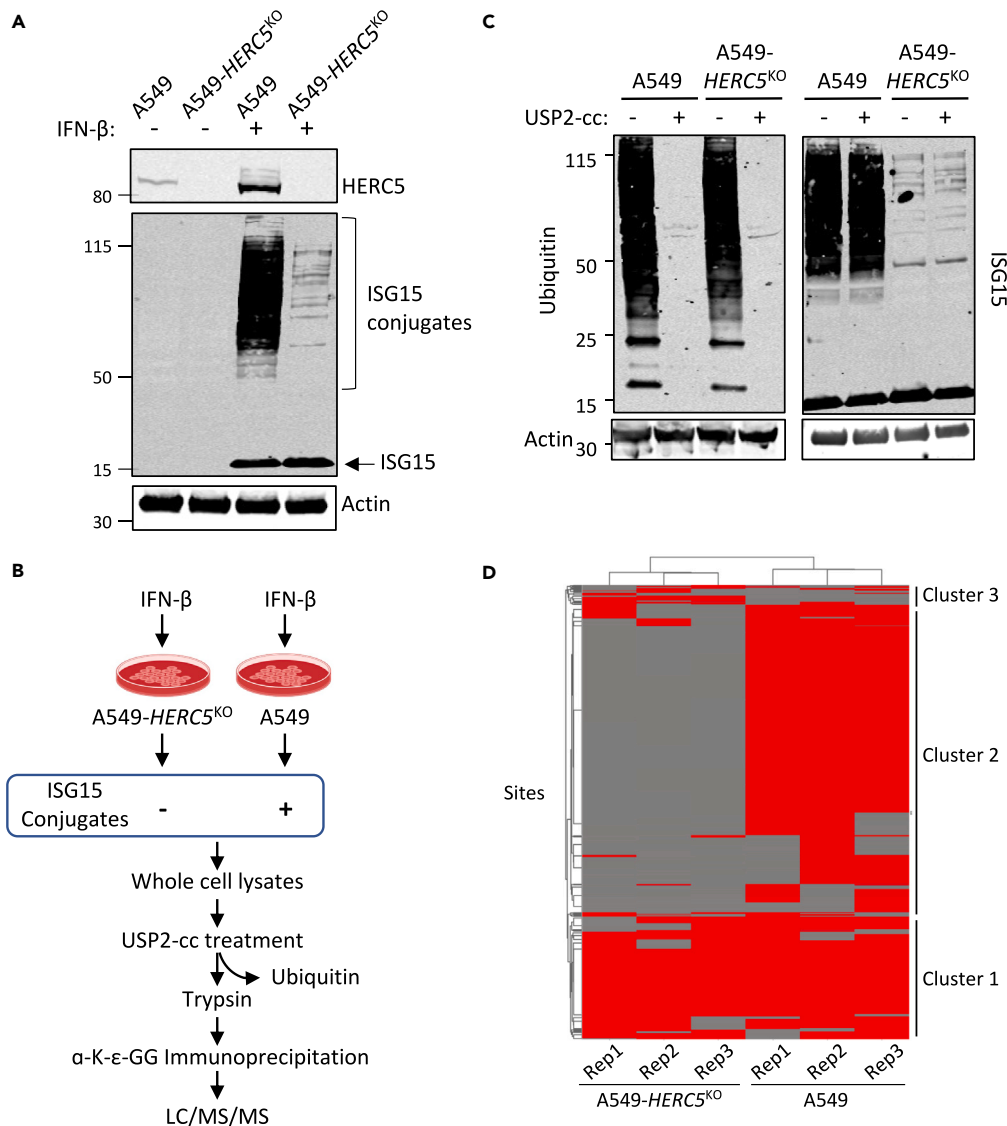


**Figure 1. Di-G proteomics of IFN- $\beta$ -treated A549 cells**

(A) A549 or A549-HERC5<sup>KO</sup> cells were treated with IFN- $\beta$  as indicated and total cell extracts were immunoblotted with antibodies specific for HERC5, ISG15, and  $\beta$ -actin.

(B) Schematic overview of the Di-G proteomics workflow for characterizing the ISGylome of IFN- $\beta$ -treated A549 cells.

(C) Cell extracts from IFN- $\beta$ -treated A549 and A549-HERC5<sup>KO</sup> cells were immunoblotted for ubiquitin (left) or ISG15 (right), before and after treatment with USP2-cc.

(D) Unsupervised clustering of 4,001 di-G peptides identified in extracts from IFN- $\beta$ -treated A549-HERC5<sup>KO</sup> and A549 cells (three replicates each).

The small amount of ISG15 conjugates present in the IFN- $\beta$ -treated A549-HERC5<sup>KO</sup> cells likely represent those catalyzed by minor ISG15 ligases (e.g., TRIM25, HHARI, and/or other unknown ligases) and/or potentially spurious ISGylation events as a consequence of the production of ISG15-charged UBE2L6 in the absence of its cognate ligase. As shown schematically in Figure 1B, A549 and A549-HERC5<sup>KO</sup> cells (90  $\times$  10 cm plates each, in three biological replicates) were treated with IFN- $\beta$  for 48 h, and total cell lysates were prepared. Lysates were treated with purified USP2-cc (catalytic core) protein, a broadly acting deubiquitinating enzyme that does not recognize ISG15 conjugates. USP2-cc reduced ubiquitin conjugates by an average of 85% across all replicates without affecting ISG15 conjugates (Figure 1C). Immunoprecipitations were then performed with anti-K- $\epsilon$ -GG antibody and peptides were processed and identified by liquid chromatography-tandem mass spectrometry (LC-MS/MS) (see STAR Methods). A total of 4,001 unique di-G modified sites met these criteria and non-supervised hierarchical clustering of these sites among the six biological samples is shown in Figure 1D. As expected, the three A549 biological replicates clustered separately from the A549-HERC5<sup>KO</sup> replicates. A significant number of sites were identified broadly across both the A549 and A549-HERC5<sup>KO</sup> replicates (cluster 1; approximately 1,000 sites) and these are expected to include residual ubiquitin and NEDD8 modification sites

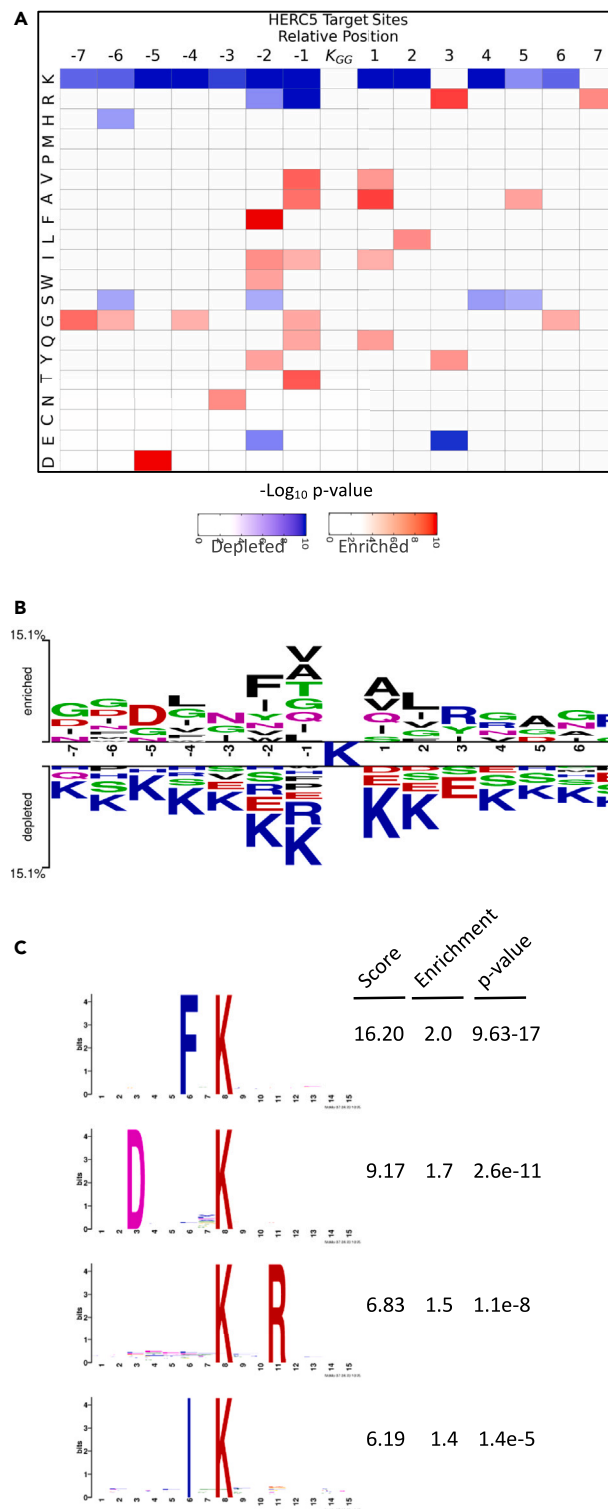


**Figure 2. Analysis of the IFN- $\beta$ -induced A549 ISGylome**

(A) Heatmap (log-transformed p values) showing the significance of overrepresentation (red) or underrepresentation (blue) for each amino acid found within +/- 7 residue window of each ISG15 modification site (2,189 sites in 1,107 proteins), relative to the amino acid frequencies within the A549 proteome. Significance was determined with two-sided Fisher's exact test and color shading represents p values  $\leq 0.001$ .

**Figure 2. Continued**

(B) Two Sample Logo showing enrichment and depletion of amino acids within  $\pm 7$  residue window of ISG15 modification sites, relative to amino acid frequencies within  $\pm 7$  residue window of all lysines in A549 proteome. Statistical significance determined by two-sample t test; p values  $\leq 0.05$ .

(C) ISGylation modification site motifs determined by MoMo. 4 of 4 returned motifs shown; full output shown in Table S7. Foreground peptides are ISG15 modification sites (2,189 sites). Background peptides represent all lysines within the A549 proteome. Motif score is sum of negative log likelihood probabilities for each residue in motif; fold enrichment over background and p values from Fisher's exact test also shown for each motif.

as well as any ISG15 sites that were independent of hHERC5 activity. Approximately 2,500 sites were specific for the A549 replicates and not found in the A549-HERC5<sup>KO</sup> replicates (cluster 2), representing hHERC5-dependent ISGylation sites. A small set of sites (500; cluster 3) were found with low reproducibility in the A549-HERC5<sup>KO</sup> replicates and were discarded. For bioinformatic analyses, we defined HERC5-dependent ISG15 modification sites as sites that were identified in at least two of the three biological replicates of the IFN-treated A549 cells (cluster 2) and were not identified in any of the three biological replicates from the A549-HERC5<sup>KO</sup> cells. Sites identified on the ISG15 conjugation enzymes, themselves (UBE1L, UBE2L6, and HERC5), were discarded, as these are likely to represent auto-ISGylation events. These filtering criteria resulted in a set of 2,189 HERC5-dependent ISG15 modification sites in IFN- $\beta$ -treated A549 cells, representing a total of 1,107 different proteins (Table S1). These proteins spanned a very wide range of categories and functions, as discussed further in the following section.

The set of ISG15 modification sites was first analyzed to determine whether hHERC5 has a preference for modifying lysines based on primary sequence context. Modified lysines were analyzed for enrichment or depletion of amino acids relative to the frequency of amino acids within the total proteome (Table S2) of IFN- $\beta$ -treated A549 cells. The window for analysis was  $\pm 7$  residues surrounding the modified lysines. Figure 2A shows a heatmap of the significance of the enrichment (red) or depletion (blue) of the twenty amino acids at each position (with p values  $< 10^{-3}$  colored and shaded). Notable features included a general depletion of other lysine residues from the  $-7$  to  $+6$  positions and a depletion of arginine at the  $-1$  and  $-2$  positions. Despite this general depletion of surrounding basic residues, there was a significant enrichment for arginine at the  $+3$  position. Alanine, valine, isoleucine, and glutamine were enriched at the  $-1$  and  $+1$  positions, and glycine was enriched at several positions on both sides of modified lysines. Aromatic residues (F, W, and Y) were enriched at the  $-2$  position and aspartic acid was enriched at  $-5$ . Figure S1A shows the representation in  $\pm 15$  residue window, demonstrating that significant enrichments and depletions fall off sharply outside of the  $\pm 7$  window. A barplot representation of the significance of enrichments and depletions for all amino acids at all positions is shown in Figure S1B, which again illustrates the general depletion of basic residues (K, R, and H) surrounding modified lysines, with the notable exception of the enrichment for arginine at  $+3$ . The enrichment for glycine at nearly all positions is also evident, as well as a general depletion of glutamic acid residues, with enrichment of aspartic acid at  $-5$ . A Two Sample Logo analysis<sup>39</sup> was also performed to visualize amino acid enrichments and depletions surrounding ISGylated lysines (Figure 2B). This again showed the general depletion of lysines surrounding the modification site as well as the enrichment of the  $-5D$ ,  $-2F$ , and  $+3R$ . MoMo (modification motifs)<sup>40</sup> is a tool for discovering motifs associated with sites of post-translational modifications. MoMo identified four statistically significant motifs, containing either  $-5D$ ,  $-2F$ ,  $-2I$ , or  $+3R$  (Figure 2C). Interestingly, none of these single amino acid enrichments were found in combination, suggesting that these represent separate and distinct preferences for hHERC5-dependent ISGylation. Together, these results indicate that hHERC5 displays preferences for lysine sequence context. At the same time, the lack of a multi-residue preferred motif suggests that hHERC5 does not have a strongly predictive recognition motif.

**Comparison of hHERC5 and mHERC6 ISGylation activities**

The set of hHERC5-dependent ISGylation sites identified in IFN- $\beta$ -treated A549 cells, described previously, represents, to our knowledge, the largest number of targets and sites attributable to a single ubiquitin or Ubl ligase, and certainly the largest set of modification sites identified for a HECT domain ligase. To further understand and expand the hHERC5-dependent ISGylome, as well as to compare hHERC5 activities to mouse HERC6 (mHERC6) activities in the same cell type, we developed a second proteomics workflow. As shown previously,<sup>10</sup> ISG15 conjugation can be recapitulated in non-IFN-treated cells by co-transfection of plasmids expressing ISG15, UBA7, UBE2L6, and HERC5. While type I IFN signaling induces all of these proteins at the transcriptional level, certain human cell lines, such as HEK293T cells, exhibit a detectable basal expression of some of these ISGs, including hHERC5. We therefore disrupted the hHERC5 gene by CRISPR in HEK293T cells in order to eliminate expression of endogenous hHERC5 and used this cell line (HEK293T-HERC5<sup>KO</sup>) for reconstitution of ISGylation by co-expression of the four ISGylation components. For hHERC5-specific di-G proteomics, 35 10-cm plates of 293T-HERC5<sup>KO</sup> cells were transfected with either a three-plasmid combination (FLAG-hISG15, hUBA7, and hUBE2L6) or four-plasmid (FLAG-hISG15, hUBA7, hUBE2L6, and hHERC5) combination, in three biological replicates. For mHERC6 proteomics, transfections were performed with plasmids expressing FLAG-mISG15, mUBE2L6, with and without mHERC6; human hUBA7 was used with the mouse ISGylation components as the E1 enzyme is not expected to influence substrate selectivity of the E3 enzymes, particularly for HECT domain ligases.<sup>41</sup> Figure 3A shows that co-expression of hHERC5 or mHERC6 with their cognate human or mouse ISG15 and E2 enzymes and hUBA7 led to the accumulation of ISG15 conjugates, and omission of either hHERC5 or mHERC6 resulted in a very low background level of ISG15 conjugation. Figure 3A also shows that treatment of the cell lysates with USP2-cc eliminated the vast majority (estimated 90%–95%) of ubiquitin conjugates and did not decrease ISG15 conjugates. Following USP2-cc treatment, lysates were digested with trypsin and di-G peptides were immunoprecipitated and processed as described previously for IFN-treated A549 cell lysates.

Co-expression of the human and mouse ISG15 conjugation components by DNA transfection in HEK293T-HERC5<sup>KO</sup> cells resulted in the identification of a total of 16,035 di-G sites across all samples. Unsupervised hierarchical clustering of these sites is shown in Figure 3B, which

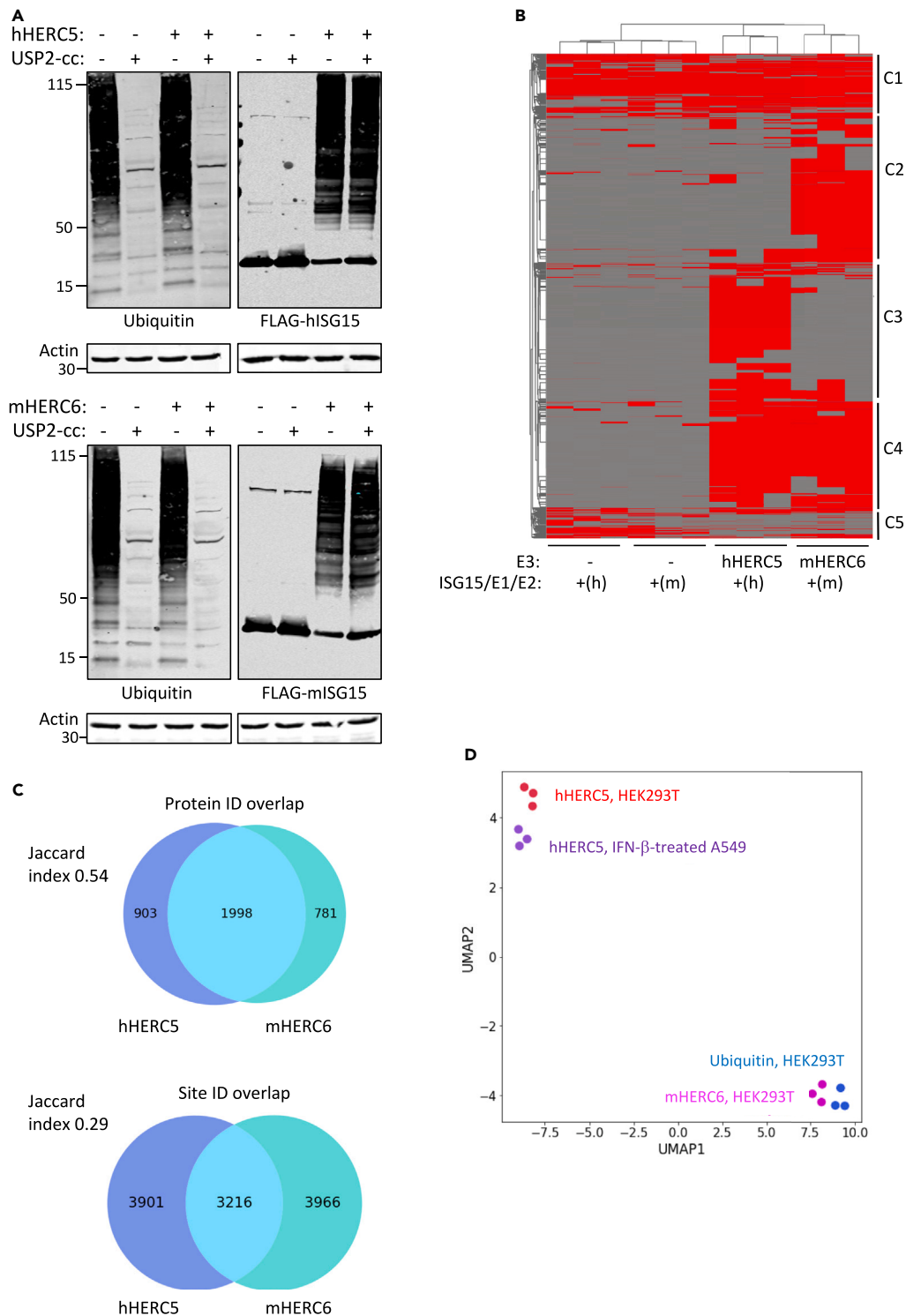


**Figure 3. Identification of targets of hHERC5 and mHERC6 by expression of conjugation components in HEK293T-HERC5<sup>KO</sup> cells**  
(A) Top: HEK293T-HERC5<sup>KO</sup> cells were transfected with plasmids expressing FLAG-hISG15, HUBA7, hUBE2L6, with or without hHERC5. Cell extracts were probed by immunoblotting for ubiquitin (left) or FLAG-ISG15 (right), before and after USP2-cc treatment. Bottom: as above, except transfected plasmids were FLAG-mISG15, HUBA7, mUBE2L6, with or without mHERC6.

**Figure 3. Continued**

(B) Unsupervised hierarchical clustering of 16,035 modified lysines identified in cells expressing the human ISGylation enzymes with and without hHERC5 and the mouse ISGylation enzymes with and without mHERC6 (three replicates of each transfection condition). Red indicates identified sites and gray indicates that the site was not identified. Five major clusters (C1-C5) are indicated; see text for complete description.

(C) Venn diagrams showing overlap of proteins that are ISGylated by hHERC5 and mHERC6 targets (left) and overlap of hHERC5 and mHERC6 ISGylation sites (right).

(D) Uniform manifold approximation and projection (UMAP) were used to visualize the lysine preferences of hHERC5 in A549 IFN- $\beta$ -induced cells (purple) and in HEK293T-transfected cells (red), as well as the lysine preferences of mHERC6 (pink) and total ubiquitylation site preferences in the HEK293T datasets (blue). Each point corresponds to one of the three experimental replicates for each condition.

identified five major clusters: sites targeted by both hHERC5 and mHERC6 (cluster 4), sites targeted by hHERC5 but not mHERC6 (cluster 3), sites targeted by mHERC6 but not hHERC5 (cluster 2), and sites that were identified across all samples (cluster 1) which likely represent Nedd8 and residual ubiquitin modification sites. A small number of sites (cluster 5) were seen with low reproducibility in the three-plasmid controls, which may represent the activity of minor ISG15 ligases and/or spurious ISGylation events as a result of the accumulation of ISG15-charged UBE2L6 proteins in the absence of a hHERC5 or mHERC6 ligase.

The di-G sites were filtered with the same criteria used for the A549 ISGylome, where hHERC5 and mHERC6 sites were considered those identified in two of three of the respective four-plasmid transfections and absent in all three of the corresponding control (three-plasmid) transfections. This resulted in a total of 2,901 proteins and 7,117 lysine residues targeted by hHERC5 (Table S3), and 2,779 proteins and 7,182 lysine residues targeted by mHERC6 (Table S4). Interestingly, the overlap of identified proteins was significantly greater than the overlap of the identified sites: ~69% of proteins targeted by hHERC5 were targeted by mHERC6 (Jaccard index of 0.54), while only ~45% of the lysines residues targeted by hHERC5 were also targeted by mHERC6 (Jaccard index of 0.29) (Figure 3C). Among the shared protein targets, 55% of the hHERC5 sites were modified by mHERC6, preliminarily suggesting that hHERC5 and mHERC6 have distinct but partially overlapping lysine selectivities.

We next determined how the hHERC5 and mHERC6 ISGylomes compared to each other and to the ubiquitylome. Di-G ubiquitin proteomics of untransfected HEK293T-*HERC5*<sup>KO</sup> cells was performed using the same workflow as described previously, with omission of the USP2-c treatment. A total of 3,672 ubiquitylation sites from 1,637 proteins (Table S5) were identified and the broad characteristics of the ubiquitylated sites were similar to those previously reported<sup>38</sup> (Figure S2A). To graphically visualize the hHERC5 and mHERC6 ISGylation preferences as well as the preferences for ubiquitylation, we created a sequence-relative-frequency vector for each dataset. This vector comprised the relative frequencies of amino acid residues at each of the  $-7/+7$  sites, and uniform manifold approximation and projection<sup>42</sup> was used to cluster and visualize the data. The three biological replicates of the A549 IFN- $\beta$  ISGylome and the HEK293T-*HERC5*<sup>KO</sup> hHERC5-transfected ISGylome replicates clustered closely together (Figure 3D), indicating that cell type differences and the method used to induce ISGylation (IFN- $\beta$  treatment or the four-plasmid transfection) did not have a significant impact on hHERC5 lysine selectivity. The mHERC6 ISGylome site preferences clustered separately from the hHERC5 preferences, supporting the conclusion that the hHERC5 and mHERC6 ligases differ in their lysine selectivities. The mHERC6 site preferences clustered closely with the ubiquitylation preferences, and a Two Sample Logo analysis within the  $+/-7$  residue window of the mHERC6 ISGylation sites and HEK293T ubiquitylation sites confirmed the overall similarity in modification sites (Figure S2B). Whether the similarities between mHERC6 site and ubiquitylation site preferences are a curiosity or of biochemical significance is unclear, as the ubiquitylation sites represent the average weighted activities of hundreds of ubiquitin ligases.

The primary sequence context of hHERC5 and mHERC6 modification sites was analyzed as described previously, relative to the amino acid frequencies within the total proteome of HEK293T cells (total HEK293T proteome presented in Table S6). As expected, properties of hHERC5-modified lysines in transfected HEK293T-*HERC5*<sup>KO</sup> cells closely resembled those seen in IFN- $\beta$ -treated A549 cells (Figure S2C; note, in particular, frequencies of K, R, F, E, and G relative to their frequencies in the proteome). Figures 4A and 4B show heatmaps for the enrichment and depletion of residues surrounding the modified lysines for the HEK293T hHERC5 and mHERC6 datasets. Notable differences between the hHERC5 and mHERC6 datasets included the following: (1) hHERC5 exhibited an overrepresentation of positively charged amino acids (K, R, and H) at position +1 to +3 relative to mHERC6, (2) hHERC5 showed a significant enrichment of all three aromatic residues (F, Y, and W) at the  $-2$  position relative to mHERC6, and (3) mHERC6 showed an enrichment of negatively charged residues (D and E) across nearly the entire window ( $-6$  to  $+7$ ) window relative to hHERC5. Notable similarities included (1) a general depletion of positively charged amino acids on the N-terminal side of the modified sites, (2) an enrichment of glycine residues at several positions on both sides of modified lysines, (3) an enrichment of uncharged amino acids at the  $-1$  and  $+1$  positions, and (4) a depletion of proline at the  $-1$  position. Two Sample Logo analysis (Figure 4B) showed that the hHERC5 enrichments and depletions were similar to those seen in the A549 dataset (e.g., the elevated frequency of the  $-2F$  and  $+3R$ ). The mHERC6 Two Sample Logo, consistent with the heatmaps, showed a higher frequency of negatively charged residues on both sides of mHERC6-ISGylated lysines relative to hHERC5 modification sites and did not show the  $-2F$  or  $+3R$  seen with hHERC5. MoMo identified several low information content motifs for both the hHERC5 and mHERC6 datasets (Figure 4C). For hHERC5, these included the  $-2F$  as well as a  $-2Y$  motif and two variations of the  $+3R$  motif. Three mHERC6 motifs were identified, all of which contained an acidic residue upstream at the  $-1$  or  $-2$  position. Additional variations at the  $-1$  or  $+1$  positions were also identified for both mHERC5 and mHERC6, and are shown in Table S7 (along with all MoMo motifs identified within all ISGylome datasets). Together, these results are consistent with the conclusion that hHERC5 and mHERC6 have distinct but overlapping preferences for lysine ISGylation based on local sequence context.

GO enrichment analysis of the A549 and HEK293T-*HERC5*<sup>KO</sup> hHERC5- and mHERC6 ISGylomes showed that modified proteins spanned a wide range of biological and biochemical functions and were localized in many cellular compartments (Figure S3A). KEGG pathway annotation

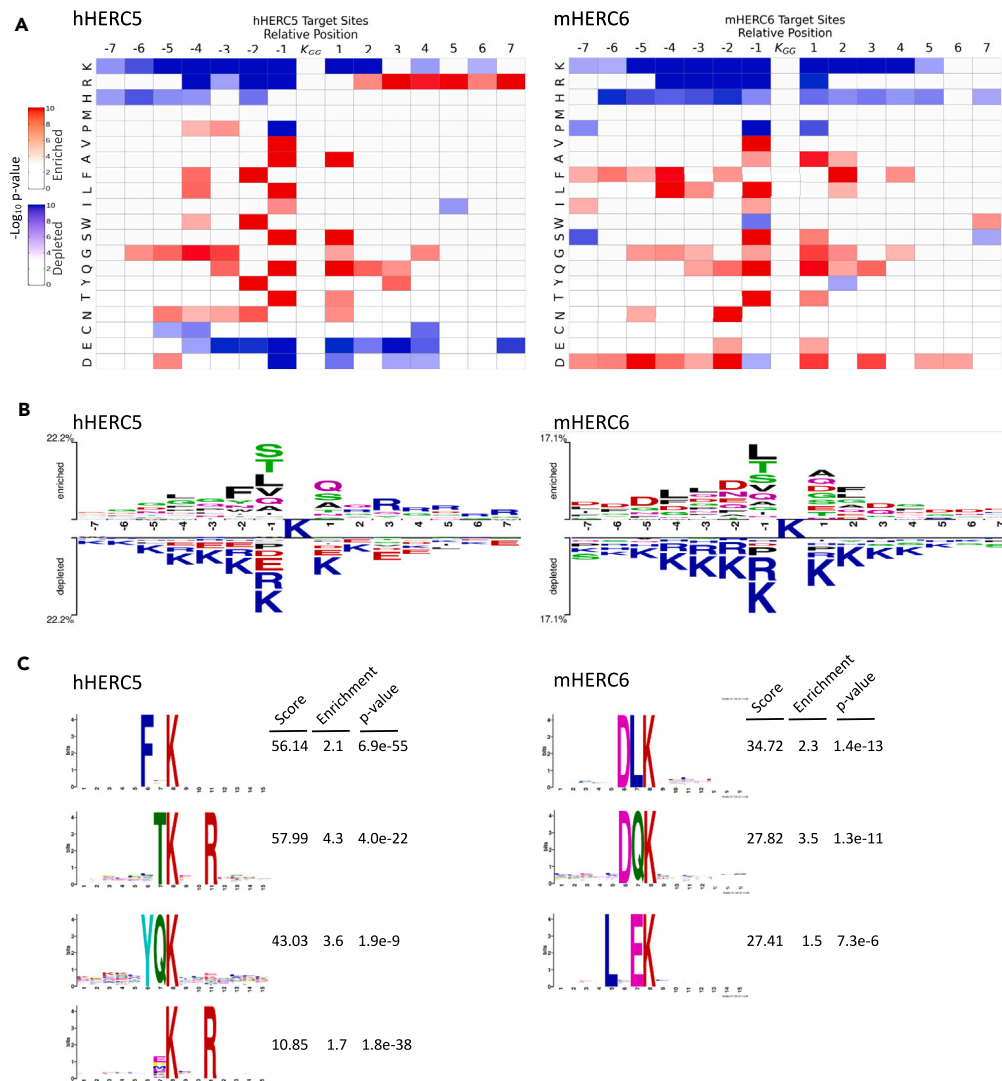


**Figure 4. Comparisons of hHERC5 and mHERC6 ISGylomes**

(A) Heatmaps (log-transformed p values) are shown for the significance of overrepresentation (red) or underrepresentation (blue) for each amino acid found within  $\pm 7$  residue window of each ISG15 modification site for the hHERC5 dataset (left) and mHERC6 dataset (right), relative to the amino acid frequencies within the HEK293T proteome. Significance was determined with two-sided Fisher's exact test and color shading represents p values  $\leq 0.001$ .

(B) Two Sample Logo showing enrichment and depletion of amino acids within  $\pm 7$  residue window of each ISG15 modification site, relative to amino acid frequencies within  $\pm 7$  residue window of all lysines in HEK293T proteome. Statistical significance determined by two-sample t test; all shown residues have p value  $\leq 0.05$ .

(C) ISGylation modification site motifs determined by MoMo. Four of 26 returned motifs shown for hHERC5, 3 of 23 shown for mHERC6. Full results shown in Table S7. Foreground peptides are ISG15 modification sites (7,117 sites for hHERC5, 7,182 sites for mHERC6). Background peptides extracted from  $\pm 7$  residue window surrounding all lysines within HEK293T proteome. Motif score is sum of negative log likelihood probabilities for each residue in motif; fold enrichment over background and p values from Fisher's exact test also shown for each motif.

of the A549 ISGylome indicated an enrichment of proteins in metabolic pathways (Figure S3B), including proteins within the glycolytic pathway, the tricarboxylic acid (TCA) cycle, fatty acid degradation and synthesis, pyruvate metabolism, and sugar metabolism. Strikingly, all eleven enzymes of the glycolytic pathway were substrates for ISGylation in all three ISGylome datasets, with the number of modified sites identified within these enzymes ranging from 1 to 15 (Figure S3C). The large number of glycolytic enzymes subject to ISGylation, discussed further in the following section, was reported previously in mice and linked to decreased glycolytic activity and thermogenesis in adipose tissue.<sup>43</sup> Five of the eight TCA cycle enzymes were also ISGylated in all three datasets, and every enzyme was modified in at least one dataset.

An expectation of the cotranslational model for ISGylation is that IFN-induced proteins might, themselves, be targets of ISGylation in IFN- $\beta$ -treated cells. 115 IFN-induced proteins were identified in the background proteome of IFN- $\beta$ -treated A549 cells (based on induction  $\geq$

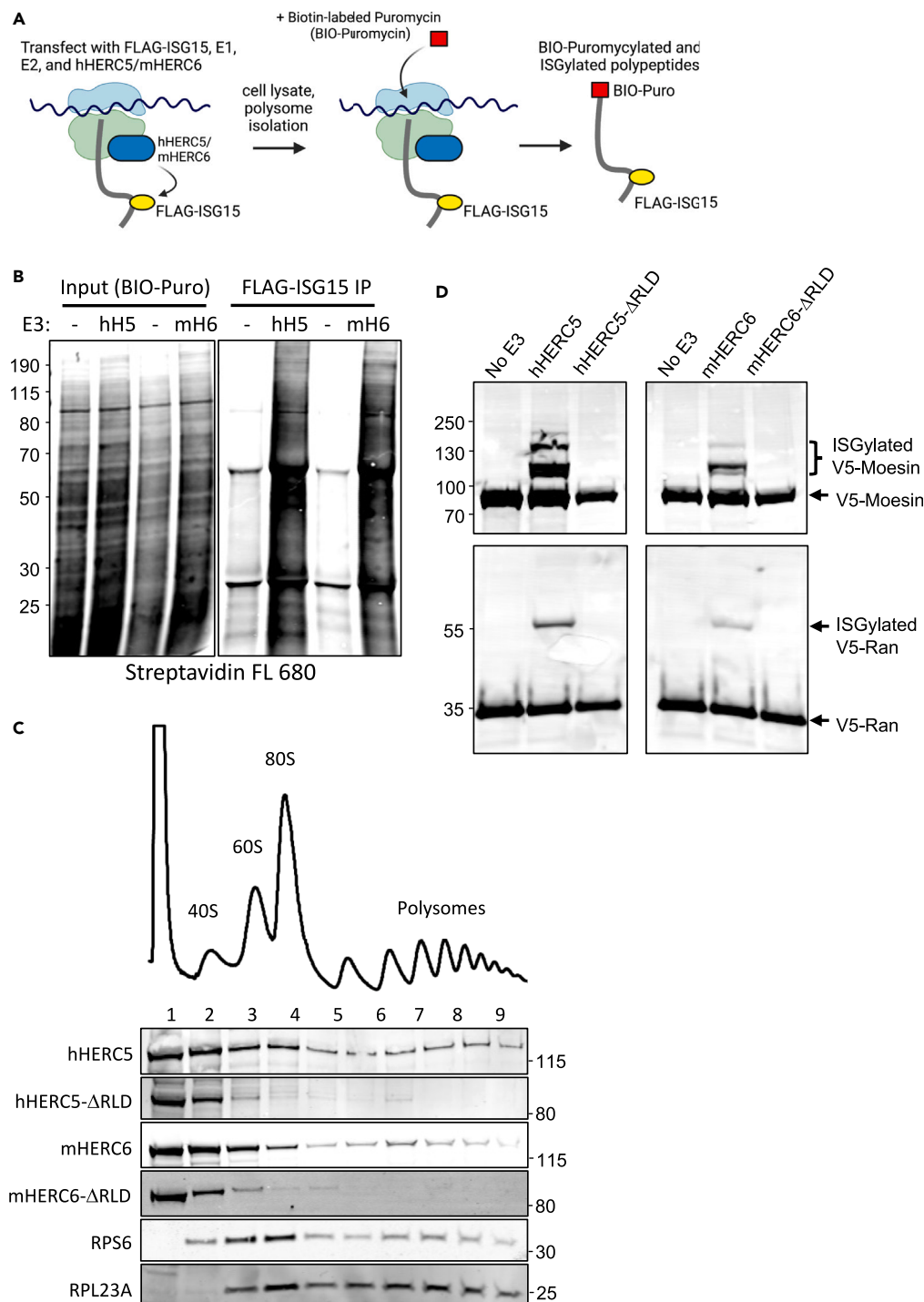


**Figure 5. Both hHERC5 and mHERC6 associate with polysomes and modify proteins cotranslationally**

(A) Schematic diagram of the cotranslational ISGylation assay. See text for complete description.

(B) Cotranslational ISGylation assay. HEK293T-HERC5<sup>KO</sup> cells were transfected with plasmids expressing hHERC5 or mHERC6 as indicated, along with hUBA7 and the respective human or mouse FLAG-ISG15 and UBE2L6 plasmids. Polysomes were isolated and nascent chains were labeled with biotinylated puromycin (Bio-Puro). The left panel shows a fraction (2.5%) of the total Bio-Puro reaction products (labeled nascent chains), detected with fluorescently labeled streptavidin (Streptavidin FL680). The right panel shows the products (biotinylated and ISGylated nascent chains) after anti-FLAG immunoprecipitation, detected with Streptavidin FL680.

**Figure 5. Continued**

(C) HEK293T-*HERC5*<sup>KO</sup> cells were transfected with plasmids expressing NTAP-tagged E3 constructs: hHERC5, hHERC5 deleted of the RCC repeat region (hHERC5- $\Delta$  RLD), mHERC6, and mHERC6- $\Delta$  RLD. Cell extracts were fractionated by sucrose density gradient ultracentrifugation and a representative A254 absorbance trace is shown (for the hHERC5 transfection), with ribosome and polysome peaks indicated. Gradient fractions were analyzed by immunoblotting with anti-protein A (to detect the NTAP tag), anti-RPS6 (small ribosomal subunit), and anti-RPL23A (large ribosomal subunit) antibodies.

(D) Deletion of the RCC repeats abrogates substrate ISGylation by both hHERC5 and mHERC6. V5-tagged Moesin or V5-Ran was expressed in HEK293T-*HERC5*<sup>KO</sup> cells as substrates for ISGylation, along with the basal ISGylation components and hHERC5, hHERC5- $\Delta$  RLD, mHERC6, or mHERC6- $\Delta$  RLD. ISGylation of the V5-tagged substrates was only detected in the presence of the full-length hHERC5 or mHERC6 proteins.

2-fold at the transcriptional level; [Interferon.org](https://www.interferon.org/)).<sup>44</sup> 40 of these proteins (~35%) were ISGylated in IFN- $\beta$ -treated A549 cells (Table S8). This was consistent with a previous smaller scale proteomics study that identified IFN-induced proteins as ISGylation targets.<sup>20</sup>

**Both hHERC5 and mHERC6 target nascent polypeptides**

We previously showed that hHERC5 associates with polysomes and broadly ISGylates newly translated proteins,<sup>28</sup> accounting for how a single ligase can target such a large number of protein targets. We developed an assay for cotranslational ISGylation (shown diagrammatically in Figure 5A) to determine if mHERC6 also functioned cotranslationally. Cells expressing FLAG-ISG15 and the E1, E2, and HERC5/6 enzymes were lysed in polysome lysis buffer containing cycloheximide and NEM; under these conditions, nascent chains are retained on polysomes at the point of cell lysis, and NEM prevents ISGylation from occurring following cell lysis. After partial purification of polysomes by sucrose density ultracentrifugation, polysomes were incubated with biotinylated puromycin (BIO-Puro), which forms a covalent bond with the terminal carboxyl group of nascent polypeptides at the peptidyl-transferase center of the ribosome. The cotranslational model for ISGylation predicts that this should result in the generation of doubly modified nascent chains (BIO-puromycylated and ISGylated), which could only have been generated if (1) hHERC5/mHERC6 ISGylated the nascent chains prior to cell lysis and (2) BIO-Puro was incorporated into those ISGylated nascent chains *in vitro* within intact translation complexes. Doubly modified products were assayed by immunoprecipitation of FLAG-ISG15 from polysome fractions followed by blotting with fluorescent streptavidin. As shown in Figure 5B, expression of the complete set of conjugation components with either hHERC5 or mHERC6 resulted in the production of the doubly modified polypeptides, while omission of hHERC5 or mHERC6 from the transfection did not result in production of the doubly modified proteins. These results indicate that both hHERC5 and mHERC6 modify nascent chains within active translation complexes.

AlphaFold<sup>13</sup>-predicted structures for hHERC5 and mHERC6 are shown in Figure S4A. Overall, the primary sequences of the proteins are 46% identical and they are 61% identical within their HECT domains. All major structural features of the two proteins are similar (the N-terminal RCC-1-like domain [RLD], central alpha-helical region, and the HECT domain; Figure S4B), with the most notable difference being the presence of an unstructured leader at the N terminus (residues 1–30) of hHERC5, prior to the RLD 7-bladed propeller structure. Deletion of the complete RLD of hHERC5 (residues 1–386) abrogates both polysome association and global ISGylation.<sup>28</sup> To determine whether the same was true for mHERC6, full-length and RLD-deletion mutants of hHERC5 and mHERC6 were expressed and assayed for co-fractionation with polysomes by sucrose density gradient ultracentrifugation. As shown in Figure 5C, a fraction of the expressed full-length hHERC5 and mHERC6 proteins co-fractionated with polysomes, while the RLD deletion mutants of both proteins were nearly completely absent from the polysome fractions. While most of the hHERC5/mHERC6 full-length proteins were not present in the polysome fractions (i.e., they remained at the top of the gradient), this was likely due to overexpression.<sup>28</sup> Both the hHERC5 and mHERC6 RLD deletion mutants were defective for protein ISGylation, as shown for two specific substrate proteins, V5-tagged Moesin and Ran (Figure 5D). Together, these results show that mHERC6 shares characteristics with hHERC5 in terms of ISGylating nascent polypeptides, associating with polysomes, and the requirement for the RLD for both polysome association and substrate protein ISGylation.

A prediction of the cotranslational model for ISGylation is that the ISGylome would be strongly biased toward more highly translated proteins. Ribosome profiling measures transcriptome-wide translation by sequencing of ribosome-protected mRNA fragments (RPFs).<sup>45</sup> A proxy of translation efficiency of specific mRNAs is then the ratio of RPF counts to mRNA abundance, as determined by RNA-seq. Three replicates of ribosome profiling and RNA-seq datasets cells were utilized to determine the translational efficiency of transcripts in HEK293T cells.<sup>46,47</sup> Of 12,374 identified transcripts, approximately 22% encoded either hHERC5 or mHERC6 targets, and the median translational efficiency of transcripts corresponding to ISG15 targets was significantly greater than for proteins that were not ISGylated (Figure 6A; Table S9). This was particularly the case for the ISGylated glycolytic and TCA cycle enzymes (Figure 6B), suggesting that the high degree of ISGylation of proteins in these pathways is due to the fact that they are simply highly translated proteins. Together, these observations are consistent with the model that the ISGylome broadly reflects the translational activity of the cell.

We also considered whether the “dwell time” of a nascent chain on the ribosome would be positively correlated with ISGylation, with the hypothesis being that the longer a lysine-containing peptide is tethered to the ribosome the greater the chance that it will be ISGylated. This would predict that longer proteins would be preferentially targeted over shorter proteins. As shown in Figure 6C, a significant difference was observed in the size distribution of proteins targeted by hHERC5 in the IFN- $\beta$ -treated A549 dataset (543 amino acids for ISGylated proteins, relative to 480 amino acids for the total proteome) and for both hHERC5 and mHERC6 in transfected HEK293T-*HERC5*<sup>KO</sup> cells (548 and 574 amino acids, respectively, relative to 480 amino acids for the proteome). This was not seen for the HEK293T ubiquitylome, where the size distribution of ubiquitylated proteins was not statistically different from that of the total proteome (Figure 6C, right).

A second prediction related to ribosome dwell time is that ISGylated lysines might be expected to be overrepresented within amino-terminal regions of proteins, as these will be exposed for a greater period of time to the activity of ribosome-bound hHERC5/mHERC6 than

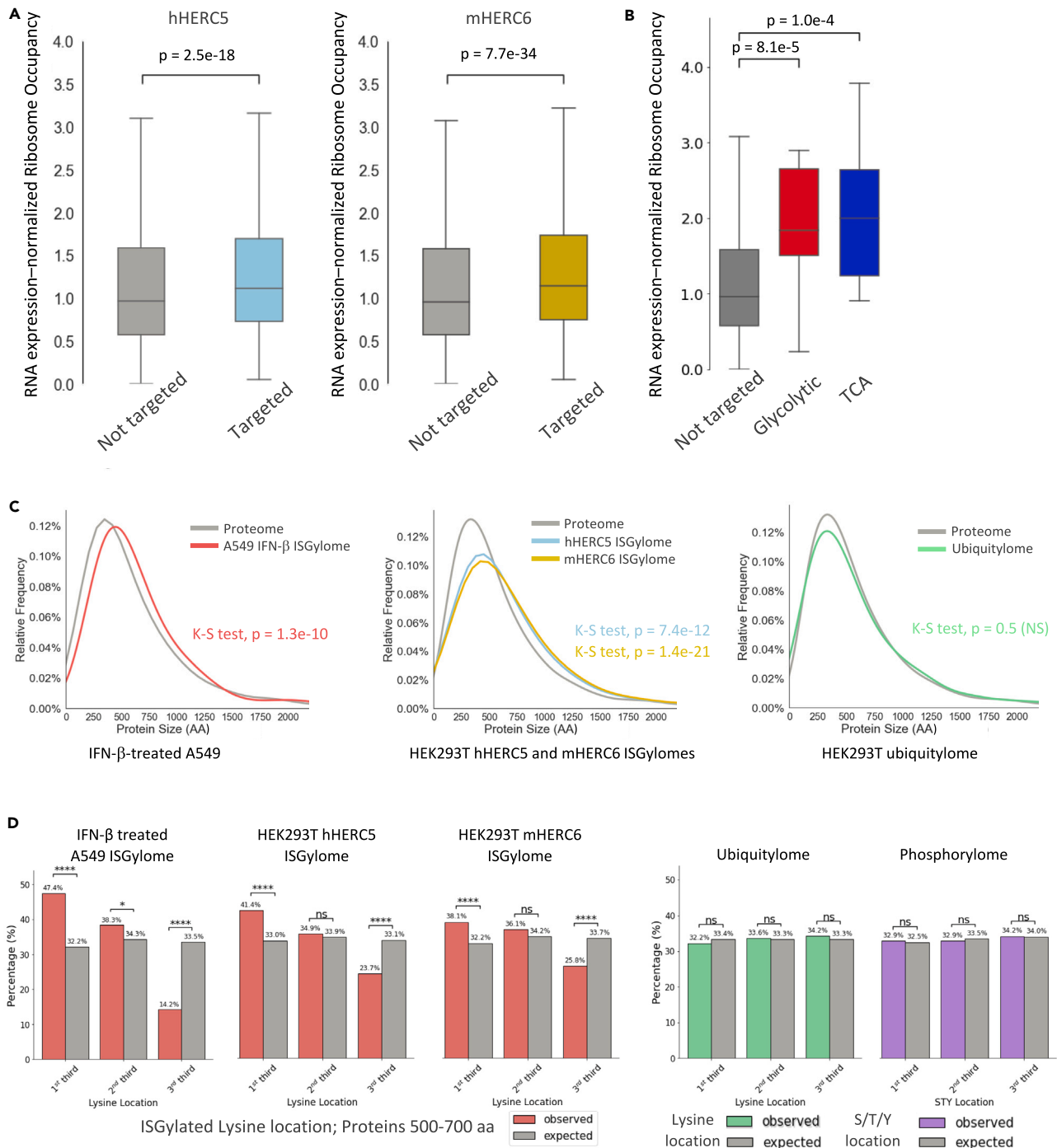


**Figure 6. Features of the hHERC5 and mHERC6 ISGylomes are consistent with cotranslational ISGylation**

(A) Boxplots comparing the distribution of the translational efficiency (RNA-expression normalized ribosome occupancy) of proteins that were not ISGylated (Not targeted) to proteins that were ISGylated (targeted) in hHERC5 and mHERC6-expressing cells. Wilcoxon rank-sum test p values are shown.

(B) Boxplot comparing the distribution of the translational efficiency of proteins that were not ISGylated (untargeted) to the translational efficiency of glycolytic enzymes (red) and TCA enzymes (blue) that were ISGylated by hHERC5 and mHERC6. Wilcoxon rank-sum test p values are shown.

(C) Left, size distribution (in number of amino acids) of proteins in the total A549 proteome (gray) and size distribution of proteins in the IFN- $\beta$ -treated A549 ISGylome (red); middle, size distribution of the total HEK293T proteome (gray) and size distribution of proteins in the HEK293T hHERC5 (blue) and mHERC6 (yellow) ISGylomes; right, size distribution of the total HEK293T proteome (gray) and the HEK293T ubiquitylome (green). Kolmogorov-Smirnov (K-S) test p values are shown.

**Figure 6. Continued**

(D) Left, distribution of sites of ISG15 modification sites on targeted proteins of (500–700) amino acids in length, in the IFN- $\beta$ -treated A549 dataset and HEK293T hHERC5 and mHERC6 datasets. Red, percentage of ISGylated lysine residues in each third of the length of the proteins; gray, percentage of total lysine residues in each third. Right, similar analysis for the HEK293T ubiquitylome (green) and phosphorylome (purple). Significance was evaluated with Z score test (\*:  $p = 0.02$ ; \*\*\*\*:  $p < 0.0001$ , ns,  $p > 0.05$ ).

lysines toward the carboxy-termini of proteins. We binned ISG15 target proteins from all three ISG15 di-G datasets into size groups of 300–500, 500–700, and 700–900 amino acids. Protein sequences within each bin were divided into thirds (N-terminal, central, and C-terminal thirds), and the distribution of ISGylated lysines within the thirds was compared to the distribution of all lysines within the same proteins. As shown in Figure 6D for proteins of 500–700 amino acids, ISGylated lysines were significantly overrepresented within the N-terminal third of the proteins and underrepresented within the C-terminal third in all three ISG15 di-G datasets. This N-terminal bias was not observed for ubiquitylation (HEK293T ubiquitylome) or an available phosphoproteome dataset,<sup>48</sup> as expected for post-translational modifications (PTMs) that occur primarily after protein synthesis is fully completed. The same results were observed for proteins of 300–500 and 700–900 amino acids in length (Figures S5A and S5B, respectively).

PTMs that occur on fully folded proteins are generally expected to be on surface-exposed residues. Although charged residues are more often surface exposed than buried in fully folded proteins, lysines can be buried or partially buried.<sup>49</sup> We reasoned that at least some lysines that are buried or partially buried in fully folded proteins might be solvent exposed during translation and therefore subject to potential ISGylation. Relative accessible surface area (RASA) is a measure of the solvent-accessible surface area of a residue within a folded protein.<sup>50</sup> It is the ratio of the solvent exposure of a residue within a folded protein to the maximum solvent exposure for that amino acid type; the RASA of a fully buried residue would be close to zero, while it would be close to one for a fully solvent-exposed residue. The RASA of each lysine residue within all ISGylated proteins was determined by Define Secondary Structure of Proteins,<sup>51,52</sup> using AlphaFold2-predicted structures of the ISGylated proteins, and the RASAs of ISGylated lysines were compared to those of the non-ISGylated lysines. As shown in Figure 7A, the median RASA of ISGylated lysines was lower than the median RASA for non-ISGylated lysines within the same proteins, for both the hHERC5 and mHERC6 datasets. In contrast, ubiquitylated lysines had a slightly higher RASA relative to all lysines within ubiquitylated proteins. Using an RASA of 0.25 as the cutoff for buried or partially buried lysines,<sup>53</sup> approximately 12.1% of all lysines had an RASA of less than 0.25, while approximately 18.5% of all ISGylated lysines had an RASA less than 0.25 (Figure 7B). By comparison, in the HEK293T ubiquitylome, approximately 11.2% of all lysines in ubiquitylated proteins had an RASA of less than 0.25, while a lower percentage (9.4%) of the ubiquitylated lysines had an RASA of less than 0.25. These results suggest that hHERC5 and mHERC6 have access to lysine residues that would be expected to be buried or partially buried in fully folded proteins, perhaps due to their exposure during translation.

## DISCUSSION

The proteomics results presented highlight several important aspects of the function of hHERC5 and mHERC6 in ISG15 conjugation, including (1) the remarkable number and breadth of proteins targeted for ISGylation by both ligases, (2) similarities and differences in the local amino acid environment surrounding hHERC5 and mHERC6 ISGylation sites, and (3) the cotranslational nature of hHERC5- and mHERC6-dependent ISGylation and the correlation of translation activity with ISGylation. In addition, the hHERC5- and mHERC6-dependent ISGylome datasets presented here represent the largest number of protein targets and modification sites attributable to a single Ub or Ubl ligase and may have implications for the lysine selectivity of HECT domain ligases, generally.

Two cell-based approaches were taken for characterizing the hHERC5 ISGylome, purifying ISG15 conjugates from either (1) an IFN- $\beta$ -treated cell line (A549) or (2) from non-IFN-treated HEK293T cells that co-expressed the four ISGylation components by DNA transfection (ISG15/E1/E2/E3). The ISGylomes from the two systems were similar to each other based on all criteria analyzed, providing an internal validation that re-constitution of ISGylation in non-IFN-treated cells did not skew the lysine selectivity of HERC5 relative to IFN- $\beta$  treatment. A comparison to mHERC6 in the same HEK293T-HERC5<sup>-/-</sup> cells allowed us to directly compare mHERC6 activity with hHERC5 (in combination with their respective human or mouse E2s and ISG15s). Interestingly, the mHERC6 +/-7 amino acid heatmap was dissimilar to the hHERC5 map in several aspects and overall was more similar to the ubiquitylome heatmap. The specific differences included enrichment of an R at the +3 position and F at the -2 position in the hHERC5 datasets, while negatively charged residues were enriched on both sides of modified lysines in the mHERC6 dataset. Importantly, many variables can systematically skew di-G peptide identification in such datasets, including the source of the anti-K-e-GG antibody, the method of minimizing contamination of ubiquitin di-G peptides, and many other factors related to post-IP peptide processing, LC-MS/MS, and data filtering. These factors can make comparisons to other published di-G datasets problematic. For example, a recent mouse ISGylome study did not note any specific enrichment or depletion of amino acids relative to modified lysines,<sup>26</sup> with the caveat that this was not a mHERC6-specific dataset. With this consideration, a very minimal conclusion from our study is that the hHERC5 and mHERC6 ligases, when analyzed in parallel in the same cell type, are significantly different with respect to amino acid composition around modified lysines, regardless of the specific nature of these differences. At the same time, we note overall lysine selectivity within our ubiquitylome was similar to that reported by Kim et al.,<sup>38</sup> indicating that our work successfully replicated specific features of the di-G datasets reported in that study.

While both hHERC5 and mHERC6 appear to have clear lysine preferences based on sequence context, we did not identify a consensus recognition motif for ISGylation by either enzyme. Among Ubls, the best example of a sequence motif for lysine modification is that for SUMOylation ( $\Psi$ -K-x-D/E), catalyzed by the UBC9 E2 enzyme.<sup>54</sup> UBC9 directly interacts with the consensus peptide sequence, although

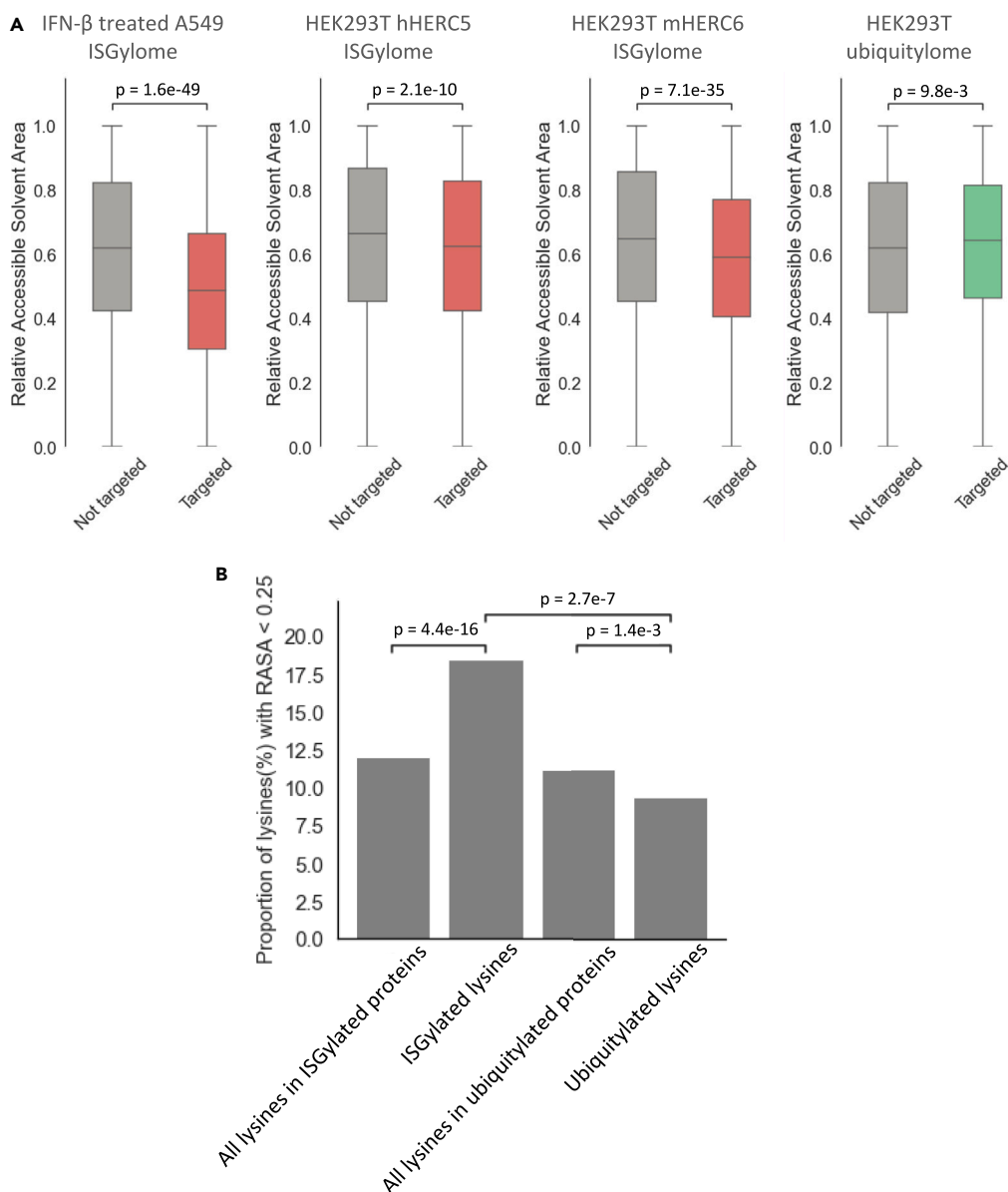


**Figure 7. Relative accessible surface area (RASA) of ISGylated and ubiquitylated lysines**

(A) Distribution of the RASAs of lysines in ISGylated proteins that are either not ISGylated (not targeted; gray bars) or ISGylated (targeted; red bars), for the IFN- $\beta$ -treated A549 ISGylome, and the HEK293T hHERC5 and mHERC6 ISGylomes. The same analysis is shown for lysines in ubiquitylated proteins that were not ubiquitylated (gray) or ubiquitylated (green) in the HEK293T ISGylome. Differences were evaluated with Wilcoxon rank-sum test; p values are shown.

(B) The percentages of lysines with an RASA < 0.25 are shown for all lysines in ISGylated proteins, all ISGylated lysines, all lysines in ubiquitylated proteins, and all ubiquitylated lysines. Fisher's exact test p values are shown.

SUMO E3s may facilitate recognition of the modification site by recruiting and orienting the UBC9, SUMO, or the substrate.<sup>55</sup> By analogy, future structural studies of the hHERC5 and mHERC6 HECT domains with peptides containing optimal modification sites might be expected to reveal the molecular basis for the lysine preferences of these ISG15 ligases. Considering the overall similarity of HECT domains, the HERC5/6 ISGylomes described here may provide a starting point for understanding lysine selectivity of HECT ubiquitin ligases, generally. It is important to note a HECT ubiquitin ligase-specific ubiquitylome would be very difficult to obtain, given the difficulty of distinguishing the targets of a single ligase from the hundreds of other ubiquitin ligases in a cell. Further, even if this were feasible, the number of substrates and sites of any single ligase would likely be too small to yield statistically significant information. The extreme number of protein targets of HERC5 and the fact that it is the single major ligase for ISG15 has provided a means for probing lysine selectivity for a HECT domain ligase. We note that Kamadurai et al.<sup>56</sup> reported on lysine prioritization of the yeast RSP5 ubiquitin ligase, although this was prioritization in the sense of spatial

location of lysine residues of the substrate, rather than sequence context of the modified lysines. Nevertheless, assay systems such as those used in that study and elsewhere, employing simplified single-lysine substrates,<sup>41,56</sup> could be adapted to address the effect of sequence context on single-lysine ubiquitylation substrates.

The vertebrate ISG15 conjugation system is remarkable for being a complete E1-E2-E3 enzyme cascade where each component is induced at the transcriptional level by type 1 interferon. Like the products of other ISGs, these proteins are involved in defense against pathogens, and in many cases viruses have evolved mechanisms to overcome or reverse ISG15 conjugation. Notable instances include influenza B, which binds and sequesters ISG15 conjugates via the NS1 protein, and viruses that encode de-ISGylating enzymes (e.g., SARS-CoV-2, FMDV, and the ERVE nairovirus).<sup>29,30,33,57</sup> On the premise that viral proteins are important targets of ISGylation, a more subtle but potentially effective approach for a virus to evade ISGylation would be to alter overall lysine content or the sequence context of lysine residues to evade the activity and inherent specificities of the HERC5/6 ISG15 ligase. Interestingly, examples of viral proteins devoid or diminished for lysine content have been noted previously, and it was suggested that this feature may have been selected for evasion of ubiquitylation;<sup>58</sup> “Lysine deserts” have also been proposed to be a basis for evasion of ubiquitylation in cellular proteins.<sup>59</sup> We suggest that such selection may also drive evasion of ISGylation for certain viral proteins. HSV-1, for example, encodes eight proteins devoid of lysines, and two of these are oligomerizing capsid proteins.<sup>58</sup> With this in mind, having a single major ligase for ISG15 would appear to be a vulnerability of the system, setting the stage for a host-pathogen evolutionary arms race where viruses are selected to evade HERC5/6 activities, while the host selects for HERC5/6 activities that will effectively combat key specific pathogens. Consistent with this, the *HERC5* gene shows evidence of pathogen-driven positive selection in primates, and the *HERC6* gene shows evidence of strong genetic selection across several mammalian orders, particularly rodents and bats.<sup>17</sup> In the case of the HERC6 proteins, the codons that show evidence of positive selection are found in all major domains of the protein (the RLD, the central domain, and the HECT domain). We speculate that some of these changes may influence lysine selectivity and may be a reflection of pressures imposed by specific pathogens over evolutionary time frames. Based on the fact that HECT domain determinants control polyubiquitin chain type formation in HECT ubiquitin ligases,<sup>41</sup> positively selected codons in HERC5/6 proteins that affect lysine selectivity might also be expected to be located within the HECT domain. Clarification of this will require biochemical characterization and roles of all the functional domains of HERC5/6 proteins. It should be noted that HERC6 in primates is also under positive selection, yet hHERC6, unlike hHERC5, does not mediate broad protein ISGylation,<sup>10</sup> suggesting that it is either a ubiquitin ligase or that it is an ISG15 ligase with a limited number of specific substrates. This underscores the importance of characterizing the HERC5 and HERC6 orthologs in other mammals, including in those few species (e.g., chinchilla and little brown bat) that encode HERC5, HERC6, and a third protein that appears to be a HERC5/6 chimera.<sup>17</sup>

We have shown here that mHERC6, like hHERC5, co-fractionates with polyribosomes, modifies nascent polypeptides within active translation complexes, and that the RLD is required for both polysome association and broad substrate ISGylation. Only a fraction of the mHERC6 protein was present in polysome sucrose gradient fractions, and this was also the case for hHERC5, as shown here and previously.<sup>28</sup> In contrast, nearly all of the endogenously expressed hHERC5 in IFN- $\beta$ -treated cells associates with polysomes,<sup>28</sup> suggesting that overexpression may saturate the capacity of hHERC5/mHERC6 to associate with polysomes. Whether other factors (other proteins or modifications of either the ligases or the ribosome) are required for association of hHERC5/mHERC6 with polysomes is not known; however, the fact that co-expression of ISG15 and the E1/E2/E3 enzymes by DNA transfection is sufficient to reconstitute ISGylation in non-IFN-treated cells indicates that any additional required factors are not induced by IFN. Consistent with a cotranslational model for ISGylation, the di-G proteomics datasets for both hHERC5 and mHERC6 showed a bias for modifying lysines within more N-terminal regions of proteins as well as a bias for modifying longer proteins relative to the total proteome. Neither of these biases were seen for global ubiquitylation. We suggest that the ISGylation biases reflect the length of time that lysines within nascent polypeptides are held in proximity to ribosome-tethered hHERC5/mHERC6 (i.e., the “dwell time” of the nascent polypeptide on the ribosome). Further biochemical evidence that hHERC5 and mHERC6 modify nascent polypeptides comes from the cotranslational ISGylation assay that detected doubly modified (ISGylated and puromycylated) polypeptides.

Post-translational modifications that occur on fully folded proteins are expected, in the vast majority of cases, to occur on surface-exposed residues. A prediction of the cotranslational model, however, is that lysines that are buried or partially buried in a fully folded protein should be accessible for modification during translation. Consistent with this, we found that the percentage of ISGylated lysines with a RASA of less than 0.25, corresponding to buried or partially buried residues, was significantly greater than the overall occurrence of buried or partially buried lysines in the same proteins. Cotranslational ISGylation, occurring prior to the completion of protein folding, is a plausible mechanism by which these lysines could have been accessible to the activity of hHERC5. At the same time, we did not expect to see that low-RASA lysines would actually be preferred modification sites, as our results suggest. A possible explanation for this can be seen by examining the motif logos generated for the hHERC5 and mHERC6 datasets (Figure 4B). While leucine did not appear in the heat maps as a residue that was enriched relative to the frequency of leucine in the proteome, it was the most common or second most common residue surrounding both sides of modified lysines. Therefore, a general hydrophobic environment around lysines might account for why lysines with an RASA of less than 0.25 might be slightly preferred targets.

We previously suggested that cotranslational ISGylation of cellular proteins, in the context of a virus-induced type I interferon response, may simply be a reflection of the proteins that are being most actively translated in a particular cell type.<sup>28</sup> Consistent with this, we have shown, using ribosome profiling data, that the median translational efficiency of transcripts corresponding to ISG15 targets was significantly greater than for proteins that were not ISGylated. The ISGylation of glycolytic and TCA cycle enzymes, as well as other IFN-induced proteins, are striking examples of this. It was recently reported that ISGylation of glycolytic enzymes, and LDHA in particular, has an important biological effect in beige adipose tissue in mice.<sup>43</sup> This is dependent on inflammation-driven activation of IRF3, which in turn activates expression of the ISGylation machinery. The consequence of LDHA ISGylation is a decrease in lactate production as a result of decreased flux through the

glycolytic pathway, which results in suppression of thermogenesis and diet-induced weight gain. Consistent with this, *isg15*<sup>-/-</sup> mice were found to be resistant to diet-induced obesity, which, interestingly, suggests that inhibitors of ISGylation (e.g., an inhibitor of hHERC5) might have therapeutic utility in obesity. This example illustrates that even though ISGylation may have important biological consequences under certain pathologic conditions (e.g., obesity and chronic inflammation), this may be driven simply by the fact that highly translated proteins, like glycolytic enzymes, are the targets of ISGylation (as opposed to a model where the ISG15 conjugation machinery was selected to specifically regulate glycolysis). A second potential example of this involves activation of ISGylation in cells deleted of NBS1, a component of the MRE11 DNA repair complex.<sup>60</sup> ISGylation of DNA replication fork proteins (including FEN1, TOP2A, SMC3, and VCP) was shown to mitigate DNA replication stress. All four of these replication fork proteins were identified in all three of our ISG15 di-G datasets, indicating that they are targets of hHERC5 and mHERC6 and that they are therefore most likely cotranslationally ISGylated, as opposed to being ISGylated at replication forks. As with ISGylation of glycolytic enzymes, we suggest that this is a case in which activation of near-stochastic hHERC5/mHERC6-dependent ISGylation under stress conditions can have important and unexpected downstream biological consequences. Finally, a large fraction of all IFN-induced proteins expressed in A549 cells were ISGylated (40 out of 115), as expected based on the cotranslational model. This was also observed in a previous smaller scale ISG15 proteomics study.<sup>20</sup> While this might be predicted to impair the functions of these proteins, it is interesting to note that while ISG15 is very rapidly induced by IFN- $\beta$ , the IFN induction of UBA7, UBE2L6, and HERC5 is significantly delayed,<sup>10</sup> consistent with the fact that ISG15 conjugates do not begin to peak until 18–24 h after IFN treatment.<sup>7</sup> We speculate that this delay in conjugation might be built into the ISG15 system in order to protect IFN-induced proteins expressed at earlier time points from being even more extensively ISGylated.

Many viruses are sensitive to the effects of ISG15 conjugation<sup>19</sup> and a central conclusion from the results described here is that hHERC5 has preferences for sites of modification, both in terms of lysine sequence context and location of lysines within protein substrates. These preferences may therefore influence the degree to which ISGylation of viral proteins is protective against specific virus types. *hHERC5* and *mHERC6* gene sequences are under positive genetic selection, suggesting that pathogens may be selected for their ability to evade the activities of ISG15 ligases. Biochemical characterization of the basis for differences in lysine selectivity as well as characterization of HERC5/6 orthologs in other vertebrate species will aid in testing the hypothesis that differences in ISGylation activities represent adaptations to species-specific pathogen challenges.

### Limitations of the study

A limitation of the study is that mouse cells were not used for proteomic analyses; mHERC6 was only analyzed in transfected human cells and not in interferon-stimulated mouse or transfected mouse cells, and hHERC5 was not analyzed in transfected mouse cells. This is significant because we cannot rule out that subtle differences in ribosomal proteins and/or translational regulation between mouse and human cells might skew the targets of the ligases when expressed in the non-cognate cell type. An additional limitation of the study is that preferential ISGylation motifs were not validated by mutagenesis of sequences surrounding modified lysines.

### STAR★METHODS

Detailed methods are provided in the online version of this paper and include the following:

- KEY RESOURCES TABLE
- RESOURCE AVAILABILITY
  - Lead contact
  - Materials availability
  - Data and code availability
- EXPERIMENTAL MODEL DETAILS
  - Cell lines
- METHOD DETAILS
  - CRISPR/Cas9 gene disruption
  - Induction of ISG15 conjugation by IFN- $\beta$  treatment or plasmid transfection
  - USP2 expression and purification and *in vitro* USP2 treatment
  - Lys- $\epsilon$ -GG (di-G) proteomics and data processing
  - Acquisition of HEK293T-HERC5<sup>KO</sup> ubiquitylome dataset
  - Acquisition of HEK293T-HERC5<sup>KO</sup> and A549 proteome background database
  - Cotranslational ISGylation assays
  - Determination of translational efficiency
  - Substrate ISGylation
  - Sucrose gradient fractionation
- QUANTIFICATION AND STATISTICAL ANALYSIS

### SUPPLEMENTAL INFORMATION

Supplemental information can be found online at <https://doi.org/10.1016/j.isci.2024.108820>.

## ACKNOWLEDGMENTS

This work was supported by a grant from the National Institute for Allergy and Infectious Diseases (AI096090) to J.M.H. Additional support was provided by the Department of Molecular Biosciences and the LaMontagne Center for Infectious Diseases, University of Texas at Austin. C. Cenik was supported by the Welch Foundation, grant F-2027-20230405. We thank Caleb Swaim for discussions on experimental strategy and interpretation of results and Maria Person and Michelle Gadush of the Center for Biomedical Research Support Biological Mass Spectrometry Facility (RRID:SCR\_021728) at UT-Austin for peptide identification and expert advice and guidance. Schematic diagrams and graphical abstract were created with BioRender ([BioRender.com](https://BioRender.com)).

## AUTHOR CONTRIBUTIONS

X.Z., J.M.P., P.A.F., C. Chan, F.W.M., and L.A.C. performed the experiments, contributed to experimental approach and design, and aided in interpretation of results. C. Cenik contributed to data analysis and interpretation of results. X.Z. and J.M.H. contributed to the writing of the manuscript.

## DECLARATION OF INTERESTS

The authors declare no competing interests.

Received: September 5, 2023

Revised: November 21, 2023

Accepted: January 2, 2024

Published: January 9, 2024

## REFERENCES

- Fensterl, V., and Sen, G.C. (2009). Interferons and viral infections. *Biofactors* 35, 14–20.
- Schoggins, J.W. (2019). Interferon-Stimulated Genes: What Do They All Do? *Annu. Rev. Virol.* 6, 567–584.
- Schneider, W.M., Chevillotte, M.D., and Rice, C.M. (2014). Interferon-stimulated genes: a complex web of host defenses. *Annu. Rev. Immunol.* 32, 513–545.
- Farrell, P.J., Broeze, R.J., and Lengyel, P. (1979). Accumulation of an mRNA and protein in interferon-treated Ehrlich ascites tumour cells. *Nature* 279, 523–525.
- Haas, A.L., Ahrens, P., Bright, P.M., and Ankel, H. (1987). Interferon induces a 15-kilodalton protein exhibiting marked homology to ubiquitin. *J. Biol. Chem.* 262, 11315–11323.
- Loeb, K.R., and Haas, A.L. (1992). The interferon-inducible 15-kDa ubiquitin homolog conjugates to intracellular proteins. *J. Biol. Chem.* 267, 7806–7813.
- Yuan, W., and Krug, R.M. (2001). Influenza B virus NS1 protein inhibits conjugation of the interferon (IFN)-induced ubiquitin-like ISG15 protein. *EMBO J.* 20, 362–371.
- Zhao, C., Beaudenon, S.L., Kelley, M.L., Waddell, M.B., Yuan, W., Schulman, B.A., Huijbregtse, J.M., and Krug, R.M. (2004). The UbcH8 ubiquitin E2 enzyme is also the E2 enzyme for ISG15, an IFN- $\alpha$ / $\beta$ -induced ubiquitin-like protein. *Proc. Natl. Acad. Sci. USA* 101, 7578–7582.
- Kim, K.I., Giannakopoulos, N.V., Virgin, H.W., and Zhang, D.-E. (2004). Interferon-inducible ubiquitin E2, Ubc8, is a conjugating enzyme for protein ISGylation. *Mol. Cell Biol.* 24, 9592–9600.
- Dastur, A., Beaudenon, S., Kelley, M., Krug, R.M., and Huijbregtse, J.M. (2006). Herc5, an interferon-induced HECT E3 enzyme, is required for conjugation of ISG15 in human cells. *J. Biol. Chem.* 281, 4334–4338.
- Zou, W., and Zhang, D.-E. (2006). The interferon-inducible ubiquitin-protein isopeptide ligase (E3) EFP also functions as an ISG15 E3 ligase. *J. Biol. Chem.* 281, 3989–3994.
- Okumura, F., Zou, W., and Zhang, D.-E. (2007). ISG15 modification of the eIF4E cognate 4EHP enhances cap structure-binding activity of 4EHP. *Genes Dev.* 21, 255–260.
- Jacquet, S., Pontier, D., and Etienne, L. (2020). Rapid Evolution of HERC6 and Duplication of a Chimeric HERC5/6 Gene in Rodents and Bats Suggest an Overlooked Role of HERCs in Mammalian Immunity. *Front. Immunol.* 11, 605270.
- Jumper, J., Evans, R., Pritzel, A., Green, T., Figurnov, M., Ronneberger, O., Tunyasuvunakool, K., Bates, R., Židek, A., Potapenko, A., et al. (2021). Highly accurate protein structure prediction with AlphaFold. *Nature* 596, 583–589.
- Ketscher, L., Basters, A., Prinz, M., and Knobloch, K.-P. (2012). mHERC6 is the essential ISG15 E3 ligase in the murine system. *Biochem. Biophys. Res. Commun.* 417, 135–140.
- Versteeg, G.A., Hale, B.G., van Boheemen, S., Wolff, T., Lenschow, D.J., and García-Sastre, A. (2010). Species-specific antagonism of host ISGylation by the influenza B virus NS1 protein. *J. Virol.* 84, 5423–5430.
- Oudshoorn, D., van Boheemen, S., Sánchez-Aparicio, M.T., Rajsbbaum, R., García-Sastre, A., and Versteeg, G.A. (2012). HERC6 is the main E3 ligase for global ISG15 conjugation in mouse cells. *PLoS One* 7, e29870.
- Paparišto, E., Woods, M.W., Coleman, M.D., Moghadasi, S.A., Kochar, D.S., Tom, S.K., Kohio, H.P., Gibson, R.M., Rohringer, T.J., Hunt, N.R., et al. (2018). Evolution-Guided Structural and Functional Analyses of the HERC Family Reveal an Ancient Marine Origin and Determinants of Antiviral Activity. *J. Virol.* 92, e00528-18.
- Peng, Y.-C., and Lenschow, D.J. (2018). ISG15 in antiviral immunity and beyond. *Nat. Rev. Microbiol.* 16, 423–439.
- Zhao, C., Denison, C., Huijbregtse, J.M., Gygi, S., and Krug, R.M. (2005). Human ISG15 conjugation targets both IFN-induced and constitutively expressed proteins functioning in diverse cellular pathways. *Proc. Natl. Acad. Sci.* 102, 10200–10205.
- Wong, J.J.Y., Pung, Y.F., Sze, N.S.-K., and Chin, K.-C. (2006). HERC5 is an IFN-induced HECT-type E3 protein ligase that mediates type I IFN-induced ISGylation of protein targets. *Proc. Natl. Acad. Sci.* 103, 10735–10740.
- Giannakopoulos, N.V., Luo, J.-K., Papov, V., Zou, W., Lenschow, D.J., Jacobs, B.S., Borden, E.C., Li, J., Virgin, H.W., and Zhang, D.-E. (2005). Proteomic identification of proteins conjugated to ISG15 in mouse and human cells. *Biochem. Biophys. Res. Commun.* 336, 496–506.
- Munnur, D., Teo, Q., Eggermont, D., Lee, H.H.Y., Thery, F., Ho, J., van Leur, S.W., Ng, W.W.S., Siu, L.Y.L., Beling, A., et al. (2021). Altered ISGylation drives aberrant macrophage-dependent immune responses during SARS-CoV-2 infection. *Nat. Immunol.* 22, 1416–1427.
- Pinto-Fernandez, A., Salio, M., Partridge, T., Chen, J., Vere, G., Greenwood, H., Olie, C.S., Damianou, A., Scott, H.C., Pegg, H.J., et al. (2021). Deletion of the deISGylating enzyme USP18 enhances tumour cell antigenicity and radiosensitivity. *Br. J. Cancer* 124, 817–830.
- Takeuchi, T., Inoue, S., and Yokosawa, H. (2006). Identification and Herc5-mediated ISGylation of novel target proteins. *Biochem. Biophys. Res. Commun.* 348, 473–477.
- Zhang, Y., Thery, F., Wu, N.C., Luhmann, E.K., Dussurget, O., Foeckle, M., Bredow, C., Jiménez-Fernández, D., Leandro, K., Beling, A., et al. (2019). The in vivo ISGylome links ISG15 to metabolic pathways and autophagy upon *Listeria* monocytogenes infection. *Nat. Commun.* 10, 5383.
- Zhu, C., Li, J., Tian, C., Qin, M., Wang, Z., Shi, B., Qu, G., Wu, C., and Nan, Y. (2021). Proteomic Analysis of ISGylation in

- Immortalized Porcine Alveolar Macrophage Cell Lines Induced by Type I Interferon. *Vaccines* 9, 164.
28. Durfee, L.A., Lyon, N., Seo, K., and Huibregtse, J.M. (2010). The ISG15 conjugation system broadly targets newly synthesized proteins: implications for the antiviral function of ISG15. *Mol. Cell* 38, 722–732.
  29. Zhao, C., Sridharan, H., Chen, R., Baker, D.P., Wang, S., and Krug, R.M. (2016). Influenza B virus non-structural protein 1 counteracts ISG15 antiviral activity by sequestering ISGylated viral proteins. *Nat. Commun.* 7, 12754.
  30. Frias-Staheli, N., Giannakopoulos, N.V., Kikkert, M., Taylor, S.L., Bridgen, A., Paragas, J., Richt, J.A., Rowland, R.R., Schmaljohn, C.S., Lenschow, D.J., et al. (2007). Ovarian Tumor Domain-Containing Viral Proteases Evade Ubiquitin- and ISG15-Dependent Innate Immune Responses. *Cell Host Microbe* 2, 404–416.
  31. Lindner, H. a., Lytwyn, V., Qi, H., Lachance, P., Ziomek, E., and Ménard, R. (2007). Selectivity in ISG15 and ubiquitin recognition by the SARS coronavirus papain-like protease. *Arch. Biochem. Biophys.* 466, 8–14.
  32. Mielech, A.M., Kilianski, A., Baez-Santos, Y.M., Mesecar, A.D., and Baker, S.C. (2014). MERS-CoV papain-like protease has deISGylating and deubiquitinating activities. *Virology* 450–451, 64–70.
  33. Swatek, K.N., Aumayr, M., Pruneda, J.N., Visser, L.J., Berryman, S., Kueck, A.F., Geurink, P.P., Ovaas, H., van Kuppeveld, F.J.M., Tuthill, T.J., et al. (2018). Irreversible inactivation of ISG15 by a viral leader protease enables alternative infection detection strategies. *Proc. Natl. Acad. Sci. USA* 115, 2371–2376.
  34. Dzimianski, J.V., Beldon, B.S., Daczkowski, C.M., Goodwin, O.Y., Scholte, F.E.M., Bergeron, É., and Pegan, S.D. (2019). Probing the impact of nairovirus genomic diversity on viral ovarian tumor domain protease (vOTU) structure and deubiquitinase activity. *PLoS Pathog.* 15, e1007515.
  35. Swaim, C.D., Canadeo, L.A., Monte, K.J., Khanna, S., Lenschow, D.J., and Huibregtse, J.M. (2020). Modulation of Extracellular ISG15 Signaling by Pathogens and Viral Effector Proteins. *Cell Rep.* 31, 107772.
  36. Ton, A.-T., Pandey, M., Smith, J.R., Ban, F., Fernandez, M., and Cherkasov, A. (2022). Targeting SARS-CoV-2 papain-like protease in the postvaccine era. *Trends Pharmacol. Sci.* 43, 906–919.
  37. Wagner, S.A., Beli, P., Weinert, B.T., Nielsen, M.L., Cox, J., Mann, M., and Choudhary, C. (2011). A proteome-wide, quantitative survey of in vivo ubiquitylation sites reveals widespread regulatory roles. *Mol. Cell. Proteomics* 10, M111.013284.
  38. Kim, W., Bennett, E.J., Huttlin, E.L., Guo, A., Li, J., Possemato, A., Sowa, M.E., Rad, R., Rush, J., Comb, M.J., et al. (2011). Systematic and quantitative assessment of the ubiquitin-modified proteome. *Mol. Cell* 44, 325–340.
  39. Vacic, V., Iakoucheva, L.M., and Radivojac, P. (2006). Two Sample Logo: a graphical representation of the differences between two sets of sequence alignments. *Bioinforma. Oxf. Engl.* 22, 1536–1537.
  40. Cheng, A., Grant, C.E., Noble, W.S., and Bailey, T.L. (2019). MoMo: discovery of statistically significant post-translational modification motifs. *Bioinforma. Oxf. Engl.* 35, 2774–2782.
  41. Kim, H.C., and Huibregtse, J.M. (2009). Polyubiquitination by HECT E3s and the determinants of chain type specificity. *Mol. Cell Biol.* 29, 3307–3318.
  42. Becht, E., McInnes, L., Healy, J., Dutertre, C.-A., Kwok, I.W.H., Ng, L.G., Ginhoux, F., and Newell, E.W. (2018). Dimensionality reduction for visualizing single-cell data using UMAP. *Nat. Biotechnol.* 37, 38–44.
  43. Yan, S., Kumari, M., Xiao, H., Jacobs, C., Kochumon, S., Jedrychowski, M., Chouchani, E., Ahmad, R., and Rosen, E.D. (2021). IRF3 reduces adipose thermogenesis via ISG15-mediated reprogramming of glycolysis. *J. Clin. Invest.* 131, e144888.
  44. Samarajiva, S.A., Forster, S., Auchettl, K., and Hertzog, P.J. (2009). INTERFEROME: the database of interferon regulated genes. *Nucleic Acids Res.* 37, D852–D857.
  45. Ingolia, N.T., Hussmann, J.A., and Weissman, J.S. (2019). Ribosome Profiling: Global Views of Translation. *Cold Spring Harb. Perspect. Biol.* 11, a032698.
  46. Ozadam, H., Geng, M., and Cenik, C. (2020). RiboFlow, RiboR and RiboPy: an ecosystem for analyzing ribosome profiling data at read length resolution. *Bioinforma. Oxf. Engl.* 36, 2929–2931.
  47. Rao, S., Hoskins, I., Tonn, T., Garcia, P.D., Ozadam, H., Sarinay, Cenik, E., and Cenik, C. (2021). Genes with 5' terminal oligopyrimidine tracts preferentially escape global suppression of translation by the SARS-CoV-2 Nsp1 protein. *RNA N. Y. N* 27, 1025–1045.
  48. Li, Z., Li, S., Luo, M., Jhong, J.-H., Li, W., Yao, L., Pang, Y., Wang, Z., Wang, R., Ma, R., et al. (2022). dbPTM in 2022: an updated database for exploring regulatory networks and functional associations of protein post-translational modifications. *Nucleic Acids Res.* 50, D471–D479.
  49. Strickler, S.S., Gribenko, A.V., Gribenko, A.V., Keiffer, T.R., Tomlinson, J., Reihle, T., Loladze, V.V., and Makhatadze, G.I. (2006). Protein stability and surface electrostatics: a charged relationship. *Biochemistry* 45, 2761–2766.
  50. Tien, M.Z., Meyer, A.G., Sydykova, D.K., Spielman, S.J., and Wilke, C.O. (2013). Maximum allowed solvent accessibilities of residues in proteins. *PLoS One* 8, e80635.
  51. Kabsch, W., and Sander, C. (1983). Dictionary of protein secondary structure: pattern recognition of hydrogen-bonded and geometrical features. *Biopolymers* 22, 2577–2637.
  52. Touw, W.G., Baakman, C., Black, J., de Beek, T.A.H., Krieger, E., Joosten, R.P., and Vriend, G. (2015). A series of PDB-related databanks for everyday needs. *Nucleic Acids Res.* 43, D364–D368.
  53. Wong, E.T.C., So, V., Guron, M., Kuechler, E.R., Malhis, N., Bui, J.M., and Gsponer, J. (2020). Protein-Protein Interactions Mediated by Intrinsically Disordered Protein Regions Are Enriched in Missense Mutations. *Biomolecules* 10, 1097.
  54. Bernier-Villamor, V., Sampson, D.A., Matunis, M.J., and Lima, C.D. (2002). Structural basis for E2-mediated SUMO conjugation revealed by a complex between ubiquitin-conjugating enzyme Ubc9 and RanGAP1. *Cell* 108, 345–356.
  55. Reverter, D., and Lima, C.D. (2005). Insights into E3 ligase activity revealed by a SUMO-RanGAP1-Ubc9-Nup358 complex. *Nature* 435, 687–692.
  56. Kamadurai, H.B., Qiu, Y., Deng, A., Harrison, J.S., Macdonald, C., Actis, M., Rodrigues, P., Miller, D.J., Souphron, J., Lewis, S.M., et al. (2013). Mechanism of ubiquitin ligation and lysine prioritization by a HECT E3. *Elife* 2, e00828.
  57. Klemm, T., Ebert, G., Calleja, D.J., Allison, C.C., Richardson, L.W., Bernardini, J.P., Lu, B.G., Kuchel, N.W., Grohmann, C., Shibata, Y., et al. (2020). Mechanism and inhibition of the papain-like protease, PLpro, of SARS-CoV-2. *EMBO J.* 39, e106275.
  58. Randow, F., and Lehner, P.J. (2009). Viral avoidance and exploitation of the ubiquitin system. *Nat. Cell Biol.* 11, 527–534.
  59. Kampmeyer, C., Grønbaek-Thygesen, M., Oelerich, N., Tatham, M.H., Cagiada, M., Lindorff-Larsen, K., Boomsma, W., Hofmann, K., and Hartmann-Petersen, R. (2023). Lysine deserts prevent adventitious ubiquitylation of ubiquitin-proteasome components. *Cell. Mol. Life Sci.* 80, 143.
  60. Wardlaw, C.P., and Petrini, J.H.J. (2022). ISG15 conjugation to proteins on nascent DNA mitigates DNA replication stress. *Nat. Commun.* 13, 5971.
  61. Durfee, L.A., Kelley, M.L., and Huibregtse, J.M. (2008). The Basis for Selective E1-E2 Interactions in the ISG15 Conjugation System. *J. Biol. Chem.* 283, 23895–23902.
  62. Deutsch, E.W., Bandeira, N., Perez-Riverol, Y., Sharma, V., Carver, J.J., Mendoza, L., Kundu, D.J., Wang, S., Bandla, C., Kamatchinathan, S., et al. (2023). The ProteomeXchange consortium at 10 years: 2023 update. *Nucleic Acids Res.* 51, D1539–D1548.
  63. Ran, F.A., Hsu, P.D., Wright, J., Agarwala, V., Scott, D.A., and Zhang, F. (2013). Genome engineering using the CRISPR-Cas9 system. *Nat. Protoc.* 8, 2281–2308.
  64. Catanzariti, A.-M., Soboleva, T.A., Jans, D.A., Board, P.G., and Baker, R.T. (2004). An efficient system for high-level expression and easy purification of authentic recombinant proteins. *Protein Sci.* 13, 1331–1339.
  65. Ryu, K.-Y., Baker, R.T., and Kopito, R.R. (2006). Ubiquitin-specific protease 2 as a tool for quantification of total ubiquitin levels in biological specimens. *Anal. Biochem.* 353, 153–155.
  66. Durfee, L.A., and Huibregtse, J.M. (2012). The ISG15 conjugation system. *Methods Mol. Biol.* 832, 141–149.
  67. Klopfenstein, D.V., Zhang, L., Pedersen, B.S., Ramirez, F., Warwick Vesztrocy, A., Naldi, A., Mungall, C.J., Yunes, J.M., Botvinnik, O., Weigel, M., et al. (2018). GOATOOLS: A Python library for Gene Ontology analyses. *Sci. Rep.* 8, 10872.
  68. Chen, E.Y., Tan, C.M., Kou, Y., Duan, Q., Wang, Z., Meirelles, G.V., Clark, N.R., and Ma'ayan, A. (2013). Enrichr: interactive and collaborative HTML5 gene list enrichment analysis tool. *BMC Bioinf.* 14, 128.

## STAR★METHODS

### KEY RESOURCES TABLE

REAGENT or RESOURCE	SOURCE	IDENTIFIER
<b>Antibodies</b>		
Mouse Monoclonal Anti-Flag M2	Sigma	CAT# F1804; RRID: AB_262044
Anti-Ubiquitin	Sigma	CAT#SAB4503053; RRID: AB_10747077
Rabbit Anti-ISG15	Thermo Fisher Scientific	CAT# 703131; RRID:AB_2784562
Rabbit Anti-HERC5	Thermo Fisher Scientific	CAT# 703675; RRID:AB_2784598
Mouse Anti-beta Actin Monoclonal (AC-15)	Thermo Fisher Scientific	CAT# AM4302; RRID:AB_2536382
Mouse Anti-V5 tag (clone SV5-Pk1), Unconjugated	Bio-Rad, formerly AbD Serotec	CAT# MCA1360; RRID:AB_322378
Mouse Anti-Ribosomal Protein S6 Monoclonal Antibody, Unconjugated, Clone C-8	Santa Cruz	CAT# sc-74459; RRID:AB_1129205
RPL23A monoclonal antibody (M10), clone 3E11	Abnova	CAT# H00006147-M10; RRID:AB_1713216
Rabbit Anti-Protein-A Antibody, Unconjugated	Sigma	CAT# P3775; RRID:AB_261038
<b>Bacterial strains</b>		
<i>E. coli</i> BL21 (DE3) Electrocompetent Cells	Novagen	CAT# 69388
<b>Chemicals, peptides, and recombinant proteins</b>		
DNA Transfection Reagent	X-tremeGENE™	CAT# 6366236001
Alt-R™ S.p. Cas9 Nuclease V3	IDT	CAT# 1081059
Alt-R™ CRISPR-Cas9 tracrRNA	IDT	CAT# 1073190
Lipofectamine™ RNAiMAX Reagent	Invitrogen	CAT# 13778-150
Human Interferon-β-1b	PBL Assay Science	CAT# 11420-1
Polyethylenimine (PEI)	Polysciences	CAT# 24765
Glutathione	Thermo Scientific	CAT# 120000050
Urea	Fisher	CAT# U15-3
Dithiothreitol (DTT)	Thermo Scientific	CAT# R0861
Iodoacetamide	Sigma	CAT# I6125
Formic acid	Fisher	CAT# A117
Acetonitrile	Fisher	CAT# A955
Trifluoroacetic acid (TFA)	Fisher	CAT# A116
Lysyl Endopeptidase (Lys-C)	FUJIFILM Wako Chemicals	CAT# 129-02541
Trypsin, bovine	Sigma	CAT# T1426
Glutathione Sepharose	GE Healthcare	CAT# 17075601
Cyclohexamide (CHX)	Sigma	CAT# C7698-5G
D-Sucrose	Fisher BioReagents	CAT# BP220-212
Biotin-dC-Puromycin	Jena Bioscience	CAT# NU-925-BIO
Anti-FLAG M2 Affinity Gel	Sigma Aldrich	CAT# A2220
SUPERaseIN RNase Inhibitor	Invitrogen	CAT# AM2696
IRDye 680RD Streptavidin	Licor	CAT# 926-68079
Halt Protease and Phosphatase Inhibitor Cocktail	ThermoFisher	CAT# 78442
<b>Critical commercial assays</b>		
Sep-Pak® C18 Cartridges	Waters	CAT# WAT051910
Quantitative Colorimetric Peptide Assay Kit	Pierce™	CAT# 23275
PTMScan® Ubiquitin Remnant Motif (K-epsilon-GG) Kit	Cell Signaling Technology	CAT# 5562
High pH Reversed-Phase Peptide Fractionation Kit	Pierce™	CAT# 84868

(Continued on next page)

**Continued**

REAGENT or RESOURCE	SOURCE	IDENTIFIER
<b>Deposited data</b>		
The mass spectrometry proteomics data have been deposited to the ProteomeXchange Consortium via the PRIDE (Deutsch et al., 2023).	Proteomexchange.org	PXD044834
<b>Experimental models: Cell lines</b>		
HEK293T CRL-3216™	ATCC	CAT# CRL-3216
HEK293T-HERC5 <sup>KO</sup>	This manuscript	N/A
A549 CCL-185™	ATCC	CAT# CCL-185
A549-HERC5 <sup>KO</sup>	This manuscript	N/A
<b>Oligonucleotides</b>		
Guide RNA for HERC5 CRISPR/Cas9 deletion; HEK293T cells; 5'-GCGCAACGGGCGCTCGACCG-3'	This manuscript	N/A
Guide RNA for HERC5 CRISPR/Cas9 deletion; A549 cells; 5'-GCGAGGTGCTCCACAATCTG-3'	This manuscript	N/A
<b>Recombinant DNA</b>		
pcDNA3 hUBA7	Durfee et al. <sup>61</sup>	N/A
pcDNA3 hUBE2L6	Durfee et al. <sup>61</sup>	N/A
pFlagCMV2-UbcM8 (mUBE2L6)	Addgene	CAT# 12440; RRID: Addgene_12440
pcDNA3 mUBE2L6	This paper	N/A
pcDNA3 HA-hHERC5	Durfee et al. <sup>61</sup>	N/A
pcDNA3 HA-mHERC6	Ketscher et al. <sup>15</sup>	N/A
pcDNA3 HA-hHERC5 ΔRCC (contains residues 381-1024 of hHERC5)	Durfee et al. <sup>61</sup>	N/A
pcDNA3 HA-mHERC6 ΔRCC (contains residues 371-1003 of mHERC6)	This manuscript	N/A
pcDNA3 V5-hHERC5	This manuscript	N/A
pcDNA3 V5-mHERC6	This manuscript	N/A
pcDNA3 NTAP-hHERC5	Dastur et al. <sup>10</sup>	N/A
pcDNA3 NTAP-hHERC5 ΔRCC (contains residues 381-1024 of hHERC5)	This manuscript	N/A
pcDNA3 NTAP-mHERC6	This manuscript	N/A
pcDNA3 NTAP-mHERC6 ΔRCC (contains residues 371-1003 of mHERC6)	This manuscript	N/A
pcDNA3 6His3xFLAG-hISG15	This manuscript	N/A
pcDNA3 6His3xFLAG-mISG15	This manuscript	N/A
MLM3636 guide RNA (gRNA) expression vector	Addgene	CAT# 43860; RRID:Addgene_43860
pSpCas9(BB)-2A-Puro (PX459) V2.0	Addgene	CAT# 62988; RRID:Addgene_62988
pET28a-LIC USP2	Addgene	CAT# 36894; RRID:Addgene_36894
pGEX-6p-USP2-cc	This manuscript	N/A
pcDNA3.1	Invitrogen	CAT# V79020
<b>Software and algorithms</b>		
Proteome Discoverer v2.5	Thermo Fisher Scientific	<a href="https://thermo.flexnetoperations.com/control/thmo/login">https://thermo.flexnetoperations.com/control/thmo/login</a>
MaxQuant	Max Plank Institute of Biochemistry	<a href="https://www.maxquant.org/">https://www.maxquant.org/</a>
Python3	Python.org	<a href="https://www.python.org/">https://www.python.org/</a>
DSSP	Wolfgang Kabsch and Chris Sander	<a href="https://github.com/PDB-REDO/dssp">https://github.com/PDB-REDO/dssp</a>

(Continued on next page)

**Continued**

REAGENT or RESOURCE	SOURCE	IDENTIFIER
RiboPy	C. Cenik	<a href="https://github.com/ribosomeprofiling/riboPy">github.com/ribosomeprofiling/riboPy</a>
Goatools		<a href="https://github.com/tanghaibao/goatools">github.com/tanghaibao/goatools</a>
Enrichr	Ma'ayan Laboratory	<a href="https://maayanlab.cloud/Enrichr">https://maayanlab.cloud/Enrichr</a>
BioRender		<a href="https://BioRender.com">BioRender.com</a>

**RESOURCE AVAILABILITY**

**Lead contact**

Further information and requests for resources and reagents should be directed to and will be fulfilled by the lead contact, Jon Huibregtse ([huibregtse@austin.utexas.edu](mailto:huibregtse@austin.utexas.edu)).

**Materials availability**

All plasmids and cell lines generated in this study are available upon request from the [lead contact](#).

**Data and code availability**

- The mass spectrometry proteomics data have been deposited to the ProteomeXchange Consortium via the PRIDE<sup>62</sup> partner repository with the dataset identifier PXD044834.
- This paper does not report original code.
- Any additional information required to reanalyze the data reported in this paper is available from the [lead contact](#) upon request.

**EXPERIMENTAL MODEL DETAILS**

**Cell lines**

HEK293T (ATCC CRL-3216; human female) and A549 (ATCC CCL-185; human male) cells were obtained directly from the American Type Culture Collection. Both cell lines and all engineered variants (see [method details](#)) were grown in Dulbecco's modified Eagle's medium (DMEM) supplemented with 10% fetal bovine serum and 1% penicillin-streptomycin and grown at 37°C with 5% atmospheric CO<sub>2</sub>. All cell lines tested negative for mycoplasma contamination.

**METHOD DETAILS**

**CRISPR/Cas9 gene disruption**

CRISPR/Cas9 gene disruption of the *HERC5* gene in HEK293T cells used the MLM3636 plasmid (Addgene #43860), modified to generate Guide RNA (gRNA) (5'-GCGCAACGGGCGCTCGACCG-3'). This was cotransfected (HP DNA Transfection Reagent X-tremeGENE) with plasmid PX459 (pSpCas9(BB)-2A-Puro V2.0; Addgene #62988).<sup>63</sup> Puromycin was used for initial positive clone screening. A549-*HERC5*<sup>KO</sup> cells were generated through direct lipofection (RNAiMax, Thermo) of assembled Cas9 ribonucleoprotein (Alt-R CRISPR Systems IDT) containing gRNA with the sequence (5'-GCGAGGTGCTCCACAATCTG-3'). Clonally selected candidates of both knockout cell lines were validated by anti-*HERC5* immunoblot of IFN- $\beta$ -treated cells.

**Induction of ISG15 conjugation by IFN- $\beta$  treatment or plasmid transfection**

HEK293T-*HERC5*<sup>KO</sup> cells were transfected at ~60% confluency using polyethylenimine (PEI) at a DNA to reagent ratio of 1:5. Cells in 10 cm plates were transfected with plasmids expressing human UBA7<sup>61</sup> (1.25  $\mu$ g), human UBE2L6<sup>8,61</sup> or mouse UBE2L6 (pFlagCMV2-UbcM8, Addgene# 12440<sup>9</sup> (1.25  $\mu$ g), HA-tagged hHERC5 or mHerc6 (1.75  $\mu$ g) and 3xFLAG-tagged human or mouse ISG15 (1.75  $\mu$ g). In control transfections, empty vector pcDNA3.1 (1.75  $\mu$ g) was used in place of hHERC5 or mHerc6 expression plasmids. Thirty-five plates of HEK293T-*HERC5*<sup>KO</sup> cells were used for each transfection condition for proteomics experiments. A549 and A549-*HERC5*<sup>KO</sup> cells were ~60% confluent when treated with IFN- $\beta$  (PBL Assay Science) at a concentration of 100 units/mL for 48 h. For proteomics experiments 90 10 cm plates were used for each IFN- $\beta$ -treated sample. Cells were harvested and lysed by sonication in buffer containing 0.5% NP40, 50 mM Tris, pH 8, and 150 mM NaCl. Protein concentrations were determined by Bradford assay (Thermo Scientific).

**USP2 expression and purification and in vitro USP2 treatment**

The catalytic core of USP2 (Usp2cc)<sup>64,65</sup> was cloned into pGEX-6P-1 plasmid and then transformed into *E. coli* BL21. Expression of GST-Usp2cc was induced in a 500 mL culture with 0.1 mM Isopropyl  $\beta$ -D-1-thiogalactopyranoside (IPTG) at 30°C, 3 h. Cells were harvested and lysed in 10 mL phosphate buffer saline (PBS) containing 1% Triton X-100 (Sigma Aldrich) by sonication. GST-fused Usp2cc was purified from clarified cell lysates using glutathione Sepharose beads (GE Healthcare) at 4°C for 2 h. Purified GST-Usp2cc was eluted from Sepharose beads with

50 mM reduced glutathione, 1 mM DTT, 50 mM Tris, pH 8.5 and 100 mM NaCl at 4°C, 16 h. HEK293T or A549 cell lysates were treated with GST-Usp2cc at a final concentration of 2.5 μM at room temperature for 3 h. De-ubiquitylation was assessed by anti-ubiquitin and anti-FLAG-*ISG15* immunoblotting.

### Lys-ε-GG (di-G) proteomics and data processing

GST-Usp2cc-treated lysates were denatured with 8 M urea (Fisher). Lysates were then reduced with 5 mM DTT at room temperature for 1 h and alkylated with 14 mM iodoacetamide in a dark room for 30 min at room temperature. Samples were digested with Lys-C (Wako, Fujifilm) at an enzyme to substrate ratio of 1:100 at 37°C for 4 h followed by digestion with trypsin (Sigma Millipore) with an enzyme to substrate ratio of 1:50 at 37°C for 15 h. Tryptic digests were acidified to a pH of 2–3 with formic acid (Fisher) and cleared by centrifugation at 10,000 × g for 10 min at room temperature. The resulting cleared digest samples were desalted with C18 reverse phase cartridges (Waters). Peptide concentrations were determined with a Quantitative Colorimetric Peptide Assay (Pierce). 70 mg peptides from the HEK293T samples and 40 mg peptides from A549 samples were used as the input for processing. Samples were lyophilized, resuspended in 1X PTMScan IAP buffer (Cell Signaling Technology), and immunoprecipitated with K-ε-GG antibody (Cell Signaling Technology). Enriched peptides were concentrated with a C18 ZipTip (Millipore Sigma) and analyzed on the Dionex LC (Thermo Fisher Scientific) and Orbitrap Fusion Lumos (Thermo Fisher Scientific) for LC-MS/MS with a 180-min run time. Raw data files were analyzed using MaxQuant version 2.0.3.0 against the SwissProt human proteome and the MaxQuant protein contaminants file. Additional specific protein sequences for mISG15, mHERC6, and mUBE2L6 were added when required for the search. The following specific search parameters were included: trypsin enzyme digest, 5 mis-cleavages permitted, fixed modification of cysteine carbamidomethylation, and variable modifications of methionine oxidation, N-terminal acetylation and lysine di-G. A 1% false discovery rate was used at both the peptide and protein level. All other settings were maintained at default.

### Acquisition of HEK293T-HERC5<sup>KO</sup> ubiquitylome dataset

Thirty untransfected HEK293T-HERC5<sup>KO</sup> cell lysates and processed as described above, without USP2-cc treatment. After desalting and lyophilization, 30 mg di-Gly peptides were enriched by immunoprecipitation with K-ε-GG antibody. Samples were concentrated and run on the LC-MS/MS system as described above. Peptide and protein identification were performed and filtered as described above.

### Acquisition of HEK293T-HERC5<sup>KO</sup> and A549 proteome background database

Untransfected HEK293T-HERC5<sup>KO</sup> and IFN-β-treated A549 cell lysates and processed as described above, without USP2-cc treatment, desalting or di-Gly enrichment. Tryptic digests were fractionated using High pH Reversed-Phase Peptide Fractionation Kit into 8 fractions per sample (Pierce™). Samples were concentrated and run on the LC-MS/MS system as described above. Raw data were analyzed using MaxQuant version 2.0.3.0 as described above but with 2 mis-cleavages permitted and di-G was not included as a variable modification.

### Cotranslational ISGylation assays

For each sample, two 100mm dishes of HEK293T-HERC5<sup>KO</sup> cells were transfected at ~60% confluency using polyethylenimine (PEI) at a DNA to reagent ratio of 1:3. Transfected plasmids for each plate consisted of 1.5 μg pCDNA3-hUBA7, 1.5 μg pCDNA3 hUBE2L6, 2.5 μg pCDNA V5-hHerc5 and 2.5 μg pcDNA 6H3XF-hISG15. Twenty-four hours post-transfection, cell were rinsed with with ice-cold PBS and lysed in 3 mL ice-cold high-salt polysome lysis buffer containing 100 mM Tris (pH 7.4), 50 mM KCl, 25 mM MgCl<sub>2</sub>, 100 μg/mL cycloheximide, 1 mM DTT, 100 μM PMSF, 4 μM leupeptin, 0.3 μM aprotinin, 200 μg/mL heparin, 50 μM N-ethylmaleimide (NEM), 40 U/mL SUPERaseIN RNase Inhibitor (Invitrogen), and 1% Triton X-100 (Sigma-Aldrich). Lysates were clarified by centrifugation at 16,300 × g for 10 min at 4°C, and supernatant was loaded onto a 2 mL 35% sucrose cushion (with 10mM Tris pH 7.4, 85mM KCl, 5mM MgCl<sub>2</sub>, 50 μg/mL cycloheximide) and centrifuged for 75 min at 316,000 × g in a Beckman NVT 65.2 rotor at 4°C. Polysome-containing pellets were resuspended in 150 μL polysome buffer (10 mM Tris pH7.4, 10 mM NaCl, 3 mM MgCl<sub>2</sub>, and 0.2 mM DTT) plus 50 μL high-salt polysome lysis buffer. Polysome-associated nascent chains were labeled with biotin-puromycin (Bio-puro) *in vitro* by incubating resuspended polysomes in 400 mM KCl, and 2 μM Bio-puro at 37°C for 15 min, followed by room temperature incubation for 75 min. Reactions were diluted with an equal volume of buffer containing 0.1% NP40, 100 mM Tris, pH 7.9, 100 mM NaCl and centrifuged at 16,300 × g for 30 s to remove any precipitated material. 2.5% of the reaction was saved to run as input to assess labeling of total nascent chains; the remainder was incubated with Anti-FLAG M2 affinity gel overnight at 4°C to immunoprecipitate FLAG-ISG15 modified nascent chains. FLAG M2 beads were washed three times with 0.1% NP40 buffer and proteins were eluted from beads by adding SDS-PAGE loading buffer and boiling at 90°C for 5 min. Samples were run on a NuPAGE 4%–12% Bis-Tris gel and transferred to PVDF-FL for probing with fluorescently tagged streptavidin.

### Determination of translational efficiency

Ribosome profiling and RNA-Seq experiments were downloaded from GSE158374.<sup>47</sup> Preprocessing and alignment of sequencing data was done using RiboFlow.<sup>46</sup> RNA-seq reads and ribosome protected footprints (28–35 nucleotides) mapping to coding regions were extracted. Expressed transcripts ( $n = 12,374$ ) were defined as having counts per million greater than one in at least two libraries ( $n = 3$  biological replicates each for RNA-seq and ribosome profiling). Translation efficiency was estimated as the ratio of the mean of normalized ribosome occupancy to RNA expression. 2,753 hHERC5 and 2,645 mHERC6 targets were among the 12,374 transcripts detected in ribosome profiling and

RNA-Seq experiments. Translation efficiency of hHERC5 and mHERC6 targets were compared to remaining detected transcripts using a two-sample Wilcoxon Rank-Sum test.

### Substrate ISGylation

HEK293T-HERC5<sup>KO</sup> cells were transfected at ~60% confluency with expression plasmids for V5-tagged substrate ORFs and the ISGylation components using polyethylenimine (PEI) at a DNA to reagent ratio of 1:3. Forty-eight hours post-transfection cells were harvested and lysed in 1% NP40 lysis buffer containing 1 mM DTT, 100  $\mu$ M PMSF, 50  $\mu$ M N-ethylmaleimide (NEM), and 100X Halt Protease and Phosphatase Inhibitor Cocktail. SDS-PAGE loading buffer was added to 30 $\mu$ g total cell lysate and samples were boiled at 90°C for 5 min, run on a NuPAGE 4%–12% Bis-Tris gel and transferred to PVDF-FL for probing with anti-V5 antibody.

### Sucrose gradient fractionation

Co-fractionation of the E3 ligases with polysomes was performed as described<sup>66</sup> with minor modifications noted here. For each ligase tested, one 100 mm culture dish of HEK293T-HERC5<sup>KO</sup> cells was transfected at ~60% confluency with 3  $\mu$ g DNA using polyethylenimine (PEI) at a DNA to reagent ratio of 1:3. Cells were harvested 24-h post-transfection at 80–90% confluency by replacing the culture media with fresh media containing cycloheximide (100  $\mu$ g/mL) for 30 min. Cells were washed with ice-cold phosphate-buffered saline (PBS) containing cycloheximide (50  $\mu$ g/mL), followed by resuspension in an ice-cold polysome lysis buffer (10 mM Tris-HCl, pH 7.4, 10 mM NaCl, 3 mM MgCl<sub>2</sub>, 200  $\mu$ g/mL Heparin, 1 U/ $\mu$ l SUPERase-In (Invitrogen), and 0.5% (v/v) Triton X-100) for 10 min. Lysates were centrifuged for 10 min at 16,300  $\times$  g at 4°C, and supernatants were loaded onto linear 7%–47% (w/v) sucrose gradients containing cycloheximide (200  $\mu$ g/mL). Gradients were centrifuged at 222,000  $\times$  g for 90 min at 4°C in a Beckman SW41Ti rotor. Polysome profiles were monitored by absorbance at 254 nm, and gradient fractions were collected on an ISCO density gradient fractionator. Following fractionation, SDS-PAGE loading buffer was added to either 30  $\mu$ L (Herc5) or 45  $\mu$ L (Herc5- $\Delta$ RLD, mHerc6, mHerc6- $\Delta$ RLD) of each of nine gradient fractions and boiled at 90°C for 5 min. Samples were run on a Bolt 4%–12% Bis-Tris gel (Thermo Fisher) and transferred to Immobilon PVDF-FL (Millipore) and probed with the indicated antibodies. Detection utilized Li-Cor reagents and instrumentation.

### QUANTIFICATION AND STATISTICAL ANALYSIS

Gene Ontology Enrichment Analysis (GOEA) was performed using the goatools<sup>67</sup> with GO slim terms. Metabolic pathway annotation was performed with Enrichr<sup>68</sup> searching the KEGG 2021 human library. Significance of GO terms or pathway enrichment was performed with Fisher's exact test and adjusted with the Benjamini-Hochberg (BH) procedure. Multiple tests with BH-adjusted p value smaller than 0.05 were considered significant. Relative accessible solvent area (RASA) was determined with DSSP<sup>51</sup> and AlphaFold<sup>13</sup> predicted structures. The structures of approximately 97% of the ISGylated or ubiquitylated proteins were available on AlphaFold. The RASAs of targeted lysines residues were compared to unmodified ones using a two-sample Wilcoxon Rank-Sum test. Motif analysis of ISGylated sites was performed using MoMo,<sup>40</sup> with the motif-x algorithm and a motif width of 15 residues and a minimum occurrence of 20 and p value threshold for individual residues of  $1.0 \times 10^6$ . Motifs are ranked according to a combination of motif score and fold enrichment; precise ranking algorithm not provided by MEME Suite. Two Sample Logo was used as a visual complement to motif enrichment.<sup>39</sup> Background proteome for both MoMo analysis and Two Sample Logo visualization consists of 15-residue peptides centered on all lysines in MS-determined proteomes. Additional information for when specific tests and analysis were used can be found in [method details](#) and Figure Legends.